nature immunology

Article

https://doi.org/10.1038/s41590-023-01636-5

The malate shuttle detoxifies ammonia in exhausted T cells by producing 2-ketoglutarate

Received: 2 February 2023

Accepted: 6 September 2023

Published online: 9 October 2023

Check for updates

Nina Weisshaar[1,3], Sicong Ma[2], Yanan Ming[2], Alaa Madi[1,3], Alessa Mieg[1,3], Marvin Hering[1,3], Ferdinand Zettl[1,3], Kerstin Mohr[1], Nora Ten Bosch[1,4], Diana Stichling[1], Michael Buettner[5], Gernot Poschet[5], Glynis Klinke[5], Michael Schulz[5], Nina Kunze-Rohrbach[5], Carolin Kerber[6], Isabel Madeleine Klein[6], Jingxia Wu[2] ✉, Xi Wang[7] ✉ & Guoliang Cui[1,3,4] ✉

The malate shuttle is traditionally understood to maintain NAD^+/NADH balance between the cytosol and mitochondria. Whether the malate shuttle has additional functions is unclear. Here we show that chronic viral infections induce $CD8^+$ T cell expression of GOT1, a central enzyme in the malate shuttle. *Got1* deficiency decreased the NAD^+/NADH ratio and limited antiviral $CD8^+$ T cell responses to chronic infection; however, increasing the NAD^+/NADH ratio did not restore T cell responses. *Got1* deficiency reduced the production of the ammonia scavenger 2-ketoglutarate (2-KG) from glutaminolysis and led to a toxic accumulation of ammonia in $CD8^+$ T cells. Supplementation with 2-KG assimilated and detoxified ammonia in *Got1*-deficient T cells and restored antiviral responses. These data indicate that the major function of the malate shuttle in $CD8^+$ T cells is not to maintain the NAD^+/NADH balance but rather to detoxify ammonia and enable sustainable ammonia-neutral glutamine catabolism in $CD8^+$ T cells during chronic infection.

$CD8^+$ T cells have crucial functions in the defense against infectious diseases. After infection, antigen-specific naïve $CD8^+$ T cells undergo clonal expansion and differentiate into anti-infection effector T (T_{eff}) cells. In acute infection, $CD8^+$ memory T (T_{mem}) cells gradually mature after antigen clearance and provide long-term protection against reinfection. In chronic infection, $CD8^+$ T cells become functionally exhausted and are referred to as exhausted T (T_{ex}) cells[1]. These T cell subsets have distinct metabolic characteristics in glycolysis and oxidative phosphorylation[2,3]. The malate shuttle indirectly transports glycolysis-produced nicotinamide adenine dinucleotide hydrogen (NADH) into the mitochondria, where NADH is converted to its oxidized form, nicotinamide adenine dinucleotide (NAD^+), by oxidative phosphorylation[4]. Whether and how the malate shuttle regulates $CD8^+$ T_{ex} cell differentiation is unknown.

A key enzyme in the malate shuttle is glutamic-oxaloacetic transaminase 1 (GOT1, or aspartate aminotransferase), which generates

[1]T Cell Metabolism Group (D192), German Cancer Research Center (DKFZ), Heidelberg, Germany. [2]Institute of Health and Medicine, Hefei Comprehensive National Science Center, Hefei, China. [3]Faculty of Biosciences, Heidelberg University, Heidelberg, Germany. [4]Helmholtz Institute for Translational Oncology (HI-TRON)—A Helmholtz Institute of the DKFZ, Mainz, Germany. [5]Metabolomics Core Technology Platform, Centre for Organismal Studies (COS), Heidelberg University, Heidelberg, Germany. [6]Tissue Bank of the German Center for Infection Research (DZIF), Partner Site Heidelberg, Institute of Pathology, Heidelberg University Hospital, Heidelberg, Germany. [7]State Key Laboratory of Reproductive Medicine and Offspring Health, Nanjing Medical University, Nanjing, China. ✉e-mail: jingxia.wu@ihm.ac.cn; xiwang@njmu.edu.cn; g.cui@dkfz.de

https://doi.org/10.1038/s41590-023-01636-5

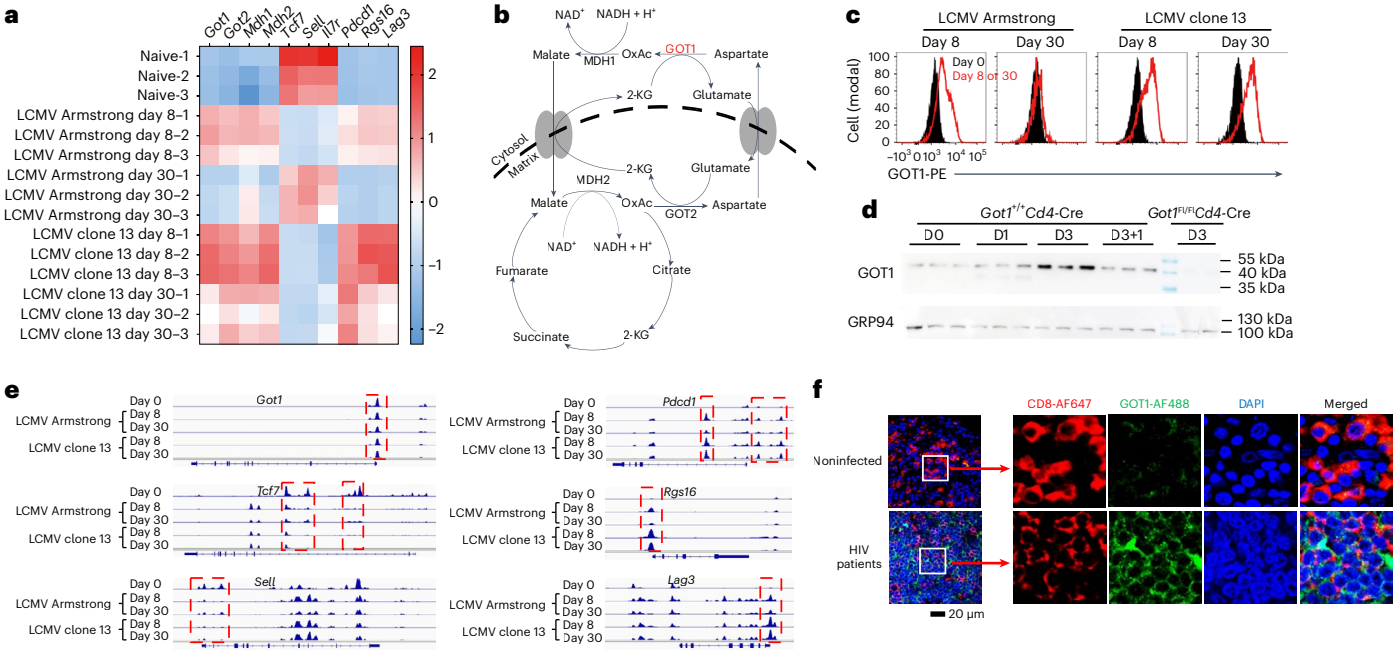

Fig. 1 | Antigenic stimulation induces GOT1 expression in human and mouse CD8$^+$ T cells. a, Heat maps show the mRNA expression *z* scores of the indicated genes in splenic LCMV $GP_{33–41}$ epitope-specific P14 CD8$^+$ T cells purified from C57BL/6 host mice after LCMV Armstrong or LCMV clone 13 infection. **b**, Illustration of the malate shuttle and TCA cycle-associated biochemical reactions. **c**, Flow cytometry histograms in red show GOT1 protein expression in P14 CD8$^+$ T cells purified from C57BL/6 host mice killed at the indicated time points after LCMV infection. Filled histograms in black 'day 0' represent P14 CD8$^+$ T cells from naïve mice and show the basal levels of GOT1 protein expression. $n = 6$ mice at each time point. **d**, *Got1*$^{+/+}$*Cd4*-Cre P14 splenocytes (*Got1*-sufficient) were cultured with $GP_{33–41}$ peptide for 1 d (D1) or 3 d (D3) before western blot analysis. On day 3, the cells were washed and cultured with IL-15 (10 ng ml^{-1}) for another day (D3 + 1). *Got1*$^{Fl/Fl}$*Cd4*-Cre P14 splenocytes (*Got1*-deficient) were included as negative controls. GRP94 was used as a loading control. $n = 3$ mice per group. Uncropped immunoblot images are shown in Source Data Fig. 8. **e**, ATAC-sequencing signal profiles across *Got1*, *Tcf7*, *Sell*, *Pdcd1*, *Rgs16* and *Lag3* loci in P14 CD8$^+$ T cells collected from naïve mice or mice infected with LCMV Armstrong or LCMV clone 13. Differentially accessible peaks are highlighted in red. Two mice were pooled in a single sample to obtain sufficient cells for analysis in the group of 'LCMV clone 13 infection day 30'. Six mice were used in total in this group. Three mice were used in each of the other groups (**a**,**e**). **f**, Immunofluorescence microscopy images show the expression of human GOT1 in CD8$^+$ T cells in lymph node sections from HIV-infected patients or donors without HIV infection. Data are representative of ten images of six donors from three independent experiments. Six-week-old male mice were used (**a**,**c**,**d**,**e**).

oxaloacetate and glutamate from 2-ketoglutarate (2-KG) and aspartate. Pharmacological inhibition of GOT1 with aminooxyacetate (AOA) affects T cell proliferation[5]. However, evidence has indicated that AOA is a pan inhibitor of pyridoxal phosphate-dependent enzymes[6–8], thus suggesting that AOA might not be suitable to specifically and accurately assess the biological function of GOT1. We used a mouse strain with T cell-specific ablation of *Got1*. We found that GOT1 catalyzed an atypical transamination chemical reaction to produce the ammonia scavenger 2-KG. CD8$^+$ T cells required GOT1 to detoxify ammonia and to catabolize glutamine in an ammonia-neutral manner when mitochondrial respiration is inhibited by chronic infection.

T cell receptor (TCR) stimulation induces GOT1 expression in CD8$^+$ T cells

To examine the potential role of the malate shuttle in antiviral CD8$^+$ T cell responses, we monitored the expression of malate shuttle-associated genes in CD8$^+$ T cells collected from mice infected with lymphocytic choriomeningitis virus (LCMV) Armstrong, which induces transient infection and acute CD8$^+$ T cell responses, or LCMV clone 13 strain, which induces persistent infection and chronic CD8$^+$ T cell responses[9]. Eight days after infection, both LCMV strains showed increased expression of genes associated with CD8$^+$ T cell activation, such as *Pdcd1*, *Rgs16* and *Lag3*, in agreement with previous findings[9]. In contrast, genes associated with T cell stemness and quiescence, such as *Tcf7*, *Sell* and *Il7r*, were expressed at lower levels in CD8$^+$ T_{eff} cells than in naïve CD8$^+$ T cells (Fig. 1a). The mRNA expression levels of genes involved in the malate shuttle, such as *Got1*, *Got2*, *Mdh1* and *Mdh2*, increased as naïve CD8$^+$ T cells differentiated into CD8$^+$ T_{eff} cells (Fig. 1a,b). Furthermore, when CD8$^+$ T_{eff} cells matured into CD8$^+$ T_{mem} cells 30 d after LCMV Armstrong infection, the expression of the malate shuttle-associated genes decreased to levels comparable to those in naïve T cells, and this response was accompanied by decreased expression of *Pdcd1*, *Rgs16* and *Lag3* and reexpression of *Tcf7*, *Sell* and *Il7r*. Persistent LCMV clone 13 infections induced and maintained the expression of *Got1*, *Got2*, *Mdh1* and *Mdh2*, in an expression pattern resembling that of *Pdcd1*, *Rgs16* and *Lag3* (Fig. 1a). The kinetics of GOT1 protein levels in virus-specific CD8$^+$ T cells was similar to that of *Got1* mRNA (Fig. 1c). Similar to the in vivo observations, TCR-transgenic P14 CD8$^+$ T cells showed significantly elevated GOT1 protein expression 3 d after cognate peptide $GP_{33–41}$ stimulation in vitro (Fig. 1d). GOT1 protein levels decreased when the $GP_{33–41}$ peptide was washed out and replaced with interleukin (IL)-15, thus suggesting that antigen persistence was required for maintaining GOT1 expression.

To further examine the potential role of TCR stimulation in driving *Got1* expression, we infected C57BL/6 mice with LCMV clone 13 or a mutated strain LCMV clone 13 V35A[10]. P14 CD8$^+$ T cells recognize the $GP_{33–41}$ epitope of LCMV clone 13, but not the mutated $GP_{33–41}$ V35A epitope of LCMV clone 13 V35A. P14 CD8$^+$ T cells in mice infected with LCMV clone 13 expressed higher levels of *Got1* than those in mice infected with LCMV clone 13 V35A, suggesting that TCR stimulation drives *Got1* expression (Extended Data Fig. 1a,b). Furthermore, we implanted C57BL/6 mice with B16 melanoma cells expressing the $GP_{33–41}$ epitope (B16-$GP_{33–41}$) or the OVA epitope (B16-OVA)[11]. Subsequently, we adoptively transferred $GP_{33–41}$ epitope-specific P14 T cells into the

tumor-bearing mice. P14 CD8$^+$ tumor-infiltrating lymphocytes recovered from B16-GP$_{33-41}$ tumors expressed significantly higher levels of *Got1* than those recovered from B16-OVA tumors, indicating that TCR stimulation induced *Got1* expression (Extended Data Fig. 1c,d).

Inhibition of the NFAT pathway significantly reduced GOT1 protein expression (Extended Data Fig. 1e,f). To test whether *Got1* is a target gene of NFAT, or other transcription factors known to regulate T cell differentiation, such as TOX, Eomes, and Blimp1, we performed chromatin immunoprecipitation (ChIP)-PCR analysis. NFAT1, TOX, Eomes and Blimp1 are known to bind to the genetic loci of *Il2* (ref. 12), *Pdcd1* (ref. 13), *Il2rb*[14] and *Id3* (ref. 15), respectively. NFAT1, but not the other three transcription factors directly bound to the −1.5 to −0.5 kb region of the *Got1* locus (Extended Data Fig. 2a–d). Taken together, these results suggested that NFAT1 bound to the *Got1* locus and promoted its expression.

The transcription initiation site (TIS) of *Got1* was constantly accessible before and after infections (Fig. 1e), thereby suggesting that LCMV infection induced the expression of *Got1* at the transcriptional level but not the epigenetic level. This mode of regulation of *Got1* expression differed from that of *Tcf7*, *Sell*, *Pdcd1*, *Rgs16* and *Lag3* (Fig. 1e). The longitudinal dynamics of chromatin accessibility of the TISs of *Sell*, *Rgs16* and *Lag3* and intron regions or intergenic regions in the *Tcf7* and *Pdcd1* loci, previously shown to be influenced by infection[16,17], mimicked their gene expression levels during the course of LCMV infection.

GOT1 protein was readily detectable in CD8$^+$ T cells from HIV-infected patients. Through confocal microscopic analysis, we observed that CD8$^+$ T cells in lymph node sections from HIV-infected patients, but not those from noninfected donors, expressed GOT1 protein (Fig. 1f). Collectively, these results suggested that both human and mouse CD8$^+$ T cells expressed GOT1 during chronic infections.

Antiviral CD8$^+$ T cell responses require GOT1 protein

To examine the potential role of GOT1 in antiviral CD8$^+$ T cell responses, we created a mouse model with T cell-specific ablation of *Got1* by breeding *Got1*$^{Flox/Flox}$ mice with the *Cd4*-Cre strain. Because CD4$^+$CD8$^+$ thymocytes give rise to mature peripheral CD4$^+$ T cells and CD8$^+$ T cells, *Cd4*-driven Cre deletes LoxP-flanked genes in both CD4$^+$ T cells and CD8$^+$ T cells[18,19]. We confirmed that the GOT1 protein was deleted through western blot analysis (Fig. 1d). *Got1*-deficient (knockout (KO)) mice had similar numbers of thymocytes, splenocytes, lymphocytes and bone marrow cells to those observed in their wild-type (WT) littermates (Extended Data Fig. 3a). *Got1* deficiency did not significantly alter the CD4$^+$ and CD8$^+$ T cell percentages among the thymocyte, splenocyte and lymphocyte populations (Extended Data Fig. 3b). Moreover, *Got1* KO and WT mice had comparable protein levels of CD44, CD62L, CD25 and IL-7Rα (Extended Data Fig. 3c–d). Collectively, *Got1* deficiency did not influence either thymic T cell development or peripheral T cell homeostasis under steady-state conditions.

To examine the potential role of GOT1 in antiviral CD8$^+$ T cell responses, we adoptively transferred *Got1* KO or WT P14 CD8$^+$ T cells into C57BL/6 host mice before LCMV clone 13 infection (Fig. 2a). The percentages of *Got1* KO donor T cells among the total CD8$^+$ T cells in the C57BL/6 host mice, as well as the absolute numbers of *Got1* KO donor T cells, were lower than those of *Got1* WT donor T cells at day 8 and day 30 after infection (Fig. 2b–d). *Got1* KO T cells expressed lower levels of inhibitory receptors, such as PD-1 and TIGIT than WT cells (Fig. 2e,f), suggesting that PD-1^{high} and TIGIT^{high} CD8$^+$ T cells were more dependent than PD-1^{low} and TIGIT^{low} CD8$^+$ T cells on GOT1. *Got1* deficiency also decreased the production of effector cytokines, IFNγ and TNF (Fig. 2g,h). Ki-67 protein levels were lower in *Got1* KO than WT CD8$^+$ T cells (Fig. 2i,j), thus suggesting that virus-specific CD8$^+$ T cells required GOT1 to proliferate during LCMV clone 13 infection. *Got1* deficiency increased the protein levels of cleaved caspase-3 and Bim (Fig. 2k,l), two proteins positively correlated with apoptosis, thereby suggesting that GOT1 promoted the survival of CD8$^+$ T cells. Together, these results indicated that GOT1 was indispensable for functional CD8$^+$ T cell survival and proliferation in the presence of persistent antigenic stimulation.

2-KG decreases the concentration of ammonia In CD8$^+$ T cells

We measured NAD$^+$, NADH and other metabolites associated with the malate shuttle (Fig. 3a–d). The NAD$^+$/NADH ratio was decreased by *Got1* deficiency in virus-specific CD8$^+$ T cells (Fig. 3b), in agreement with the widely appreciated role of the malate shuttle in maintaining the NAD$^+$/NADH balance. Supplementation with the NAD$^+$ precursor molecules nicotinamide riboside (NR) and nicotinamide mononucleotide (NMN) did not fully restore the cell numbers of *Got1* KO CD8$^+$ T cells (Fig. 3e,f), suggesting that although *Got1* deficiency disturbed the NAD$^+$/NADH balance, it was not primarily responsible for defects in *Got1* KO CD8$^+$ T cell accumulation.

Furthermore, *Got1* deficiency decreased the abundance of 2-KG and malate in CD8$^+$ T cells (Fig. 3c). Because these metabolites have been shown to regulate ammonia metabolism[20,21], we measured ammonia and observed that *Got1* deficiency significantly increased concentrations of ammonia (Fig. 3d). We quantified the mass of CD8$^+$ T cells by using graduated packed cell volume tubes. On the basis of the assumption that the major component of cells was water, the average concentrations of ammonia in *Got1*-deficient CD8$^+$ T cells exceeded 3,000 μM (calculated by dividing the total amount of ammonia by the CD8$^+$ T cell mass). The physiological concentrations of ammonium in mouse blood range from 23.8 to 76.9 μM[22]. Because ammonia has been reported to be toxic at concentrations above 1,000 μM[23], we hypothesized that the failure of ammonia removal caused *Got1* KO CD8$^+$ T cell death. Supplementation with cell membrane-permeable 2-KG and malate, particularly 2-KG, decreased the abundance of ammonia and increased the percentages of *Got1* KO CD8$^+$ T cells among all CD8$^+$ T cells (Fig. 3f). Moreover, 2-KG has been shown to activate histone demethylase[24,25] and DNA demethylase[26,27]. GSK-J4 and 2-HG, which are inhibitors of histone demethylase and DNA demethylases[28–30], did not influence the pro-survival and ammonia-decreasing effects of 2-KG (Fig. 3e,f). These results suggested that 2-KG's restoration of *Got1* KO CD8$^+$ T cell accumulation did not occur through activating histone and DNA demethylases.

Ammonia significantly inhibited the growth of *Got1* WT CD8$^+$ T cells and *Got1* KO CD8$^+$ T cells at concentrations higher than 2 mM or 0.25 mM, respectively (Fig. 3g). Ammonia (at 1 mM) did not significantly influence *Got1* WT CD8$^+$ T cell numbers at either 24 h or 48 h after treatment (Fig. 3h). In contrast, ammonia at the same concentration significantly decreased *Got1* KO CD8$^+$ T cell numbers. Ammonia treatment increased the percentages of Annexin V$^+$ propidium iodide (PI)$^+$ CD8$^+$ T cells (Extended Data Fig. 4a,c), suggesting that ammonia promotes CD8$^+$ T cell apoptosis. Additionally, ammonia inhibited the expression levels of Ki-67, and *Got1*-deficient CD8$^+$ T cells were more susceptible to ammonia-induced inhibition of cell proliferation than *Got1*-sufficient CD8$^+$ T cells (Extended Data Fig. 4b,d). Taken together, these results suggested that ammonia promoted CD8$^+$ T cell apoptosis and inhibited cell proliferation, and *Got1* deficiency further sensitized CD8$^+$ T cells to ammonia-induced apoptosis and inhibition of cell proliferation.

To examine whether 2-KG assimilated free ammonia into glutamate and, therefore, detoxified free ammonia (Fig. 3i), we cultured CD8$^+$ T cells with ^{15}N tracer-labeled NH_4Cl in the presence or absence of 2-KG. The addition of 2-KG significantly increased the amount of ^{15}N tracer-labeled glutamate, suggesting that 2-KG enhanced the assimilation of ammonia into glutamate in CD8$^+$ T cells (Fig. 3j). Together, the results indicated that GOT1 was required for CD8$^+$ T cells to generate 2-KG, which promoted the assimilation of free ammonia and cell survival.

GOT1 promotes T_{eff} cell formation in acute LCMV infection

Because the expression levels of GOT1 transiently increased on day 8 after LCMV Armstrong infection (Fig. 1c), we investigated the potential

https://doi.org/10.1038/s41590-023-01636-5

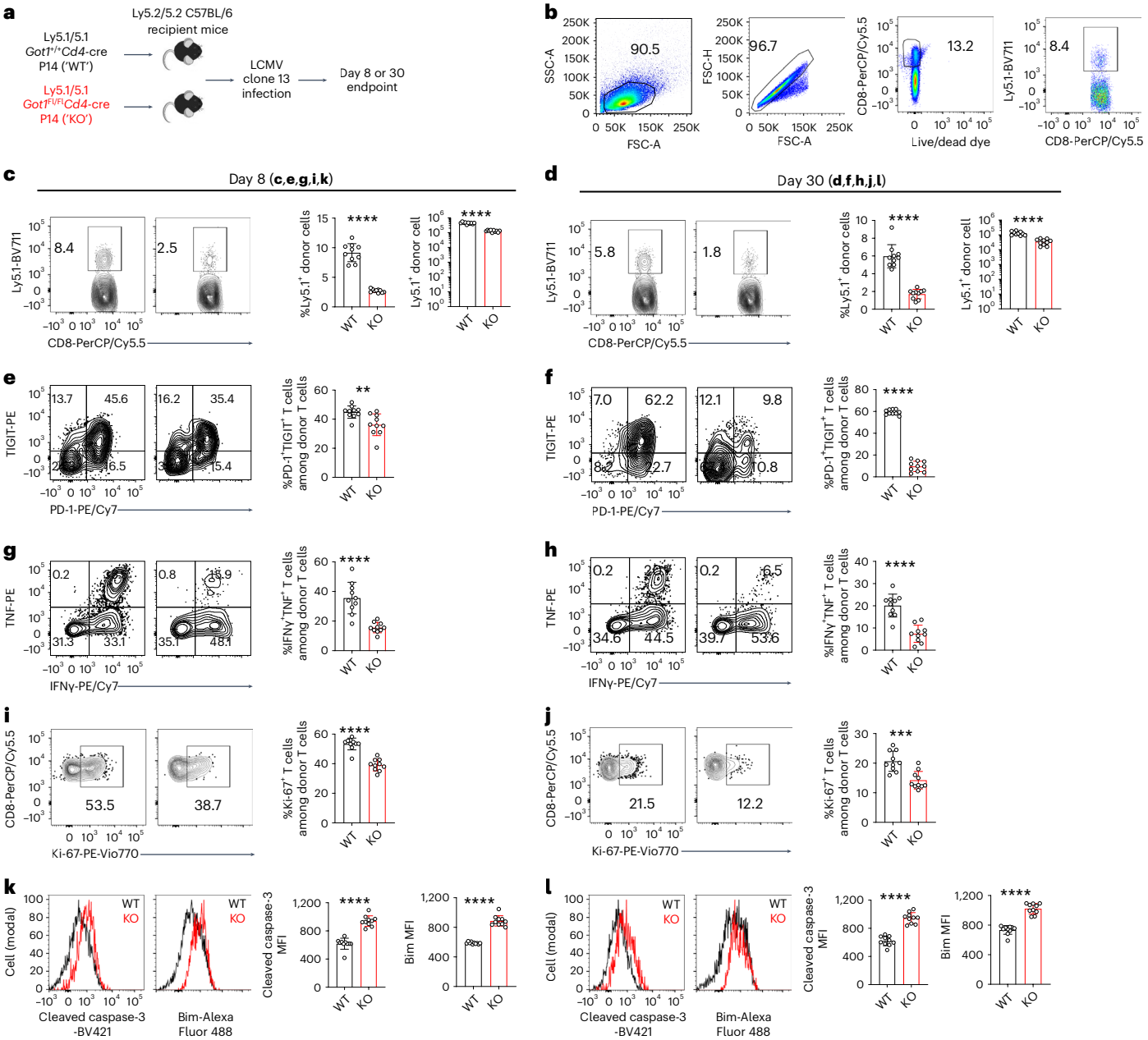

Fig. 2 | Antiviral CD8⁺ T cell responses require GOT1 during chronic infection. **a**, Illustration of the experimental design. **b**, Fluorescence-activated cell sorting (FACS) gating strategies used in **c**–**l**. **c**–**l**, Contour plots, histograms and bar graphs show the flow cytometry staining results of Ly5.1⁺ donor P14 CD8⁺ T cells (**c**,**d**), PD-1 and TIGIT (**e**,**f**), cytokines (**g**,**h**), Ki-67 (**i**,**j**) and cleaved caspase-3 and Bim (**k**,**l**) in *Got1*-deficient and sufficient P14 CD8⁺ T cells. Cells were stimulated with GP_{33-41} peptides before the flow cytometry staining (**g**–**h**). Data were pooled from two independent experiments (**c**–**l**) with ten C57BL/6 mice in each group receiving *Got1*-deficient and sufficient donor P14 CD8⁺ T cells. The results are presented as mean ± s.d. $^{**}P < 0.01$; $^{***}P < 0.001$; $^{****}P < 0.0001$. Comparisons were performed with the two-tailed Mann–Whitney test (percentage of Ly5.1⁺ donor cells in **d** and **i**, cleaved caspase-3 MFI in **k** and Bim MFI in **l**; data points were not normally distributed) or a two-tailed Student's *t*-test (other comparisons). In **c**, $P = 1.14 \times 10^{-10}$ (left) and $P = 9.48 \times 10^{-12}$ (right); in **d**, $P = 1.08 \times 10^{-5}$ (left) and $P = 9.08 \times 10^{-7}$ (right); in **e**, $P = 0.0048$; in **f**, $P = 1.0 \times 10^{-15}$; in **g**, $P = 2.47 \times 10^{-5}$; in **h**, $P = 6.99 \times 10^{-6}$; in **i**, $P = 2.17 \times 10^{-5}$; in **j**, $P = 0.0003$; in **k**, $P = 1.08 \times 10^{-5}$ (left) and $P = 8.84 \times 10^{-11}$ (right); in **l**, $P = 8.70 \times 10^{-9}$ (left) and $P = 1.08 \times 10^{-5}$ (right). Six-week-old female mice were used (**b**–**l**).

role of GOT1 in regulating the formation of effector CD8⁺ T cells during LCMV Armstrong acute infections (Extended Data Fig. 5a). *Got1* deficiency modestly but significantly reduced the numbers of virus-specific CD8⁺ T cells on day 8 but not day 30 after LCMV Armstrong infection (Extended Data Fig. 5b–d). *Got1* deficiency did not influence the protein levels of *KLRG1* or IL-7Rα (Extended Data Fig. 5e–f). *Got1* deficiency decreased effector cytokine production and cell proliferation and increased the expression levels of apoptosis-related protein markers on day 8 but not on day 30 (Extended Data Fig. 5g–l). This selective requirement of GOT1 for the accumulation of CD8⁺ T_{eff} cells on day 8, but not for the accumulation of CD8⁺ T_{mem} cells on day 30, is consistent with the selective expression of GOT1 in CD8⁺ T_{eff} cells, but only at basal levels in CD8⁺ T_{mem} cells (Fig. 1c).

In acute LCMV Armstrong infections, *Got1* deficiency significantly reduced the NAD⁺/NADH ratio (Extended Data Fig. 6a) but did not influence the abundance of ammonia (Extended Data Fig. 6b). Supplementation with the NAD⁺ precursor molecules NR and NMN, but not the ammonia scavenger 2-KG, restored numbers of

https://doi.org/10.1038/s41590-023-01636-5

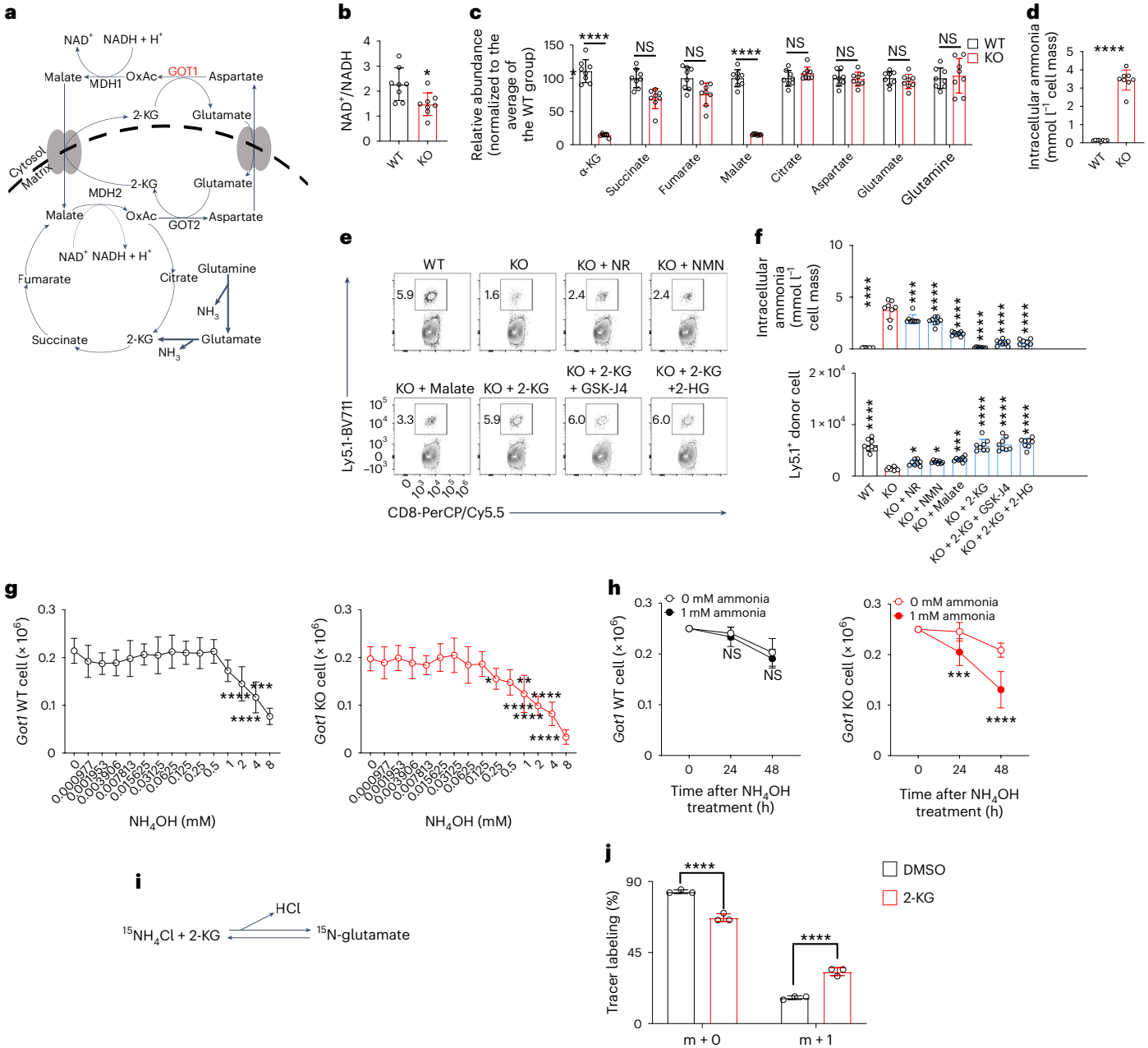

Fig. 3 | T_{ex} cells require GOT1 to accumulate 2-KG that detoxifies ammonia. **a**, The malate shuttle, TCA cycle and glutaminolysis. **b**–**d**, Bar graphs show NAD^+/NADH ratios (**b**), indicated metabolites (**c**) and ammonia (**d**) in *Got1*-deficient and sufficient donor P14 $CD8^+$ T cells isolated from C57BL/6 host mice infected 30 d earlier with LCMV clone 13. **e**,**f**, Splenocytes were isolated from host mice 30 d after infection and were cultured with GP_{33-41} peptides in the presence of the indicated compounds for 1 d. Flow cytometry contour plots show the percentages of $Ly5.1^+$ donor T cells among $CD8^+$ T cells (**e**). Bar graphs show the concentrations of ammonia in donor T cells and the numbers of T cells (**f**). **g**,**h**, *Got1*-deficient and *Got1*-sufficient donor P14 $CD8^+$ T cells were isolated from C57BL/6 host mice infected with LCMV clone 13 30 d earlier. 0.25×10^6 cells were cultured with anti-CD3 and anti-CD28 in the presence or absence of NH_4OH for 2 d. Line graphs show the number of cells after culturing with NH_4OH at the indicated concentrations (**g**) or for the indicated time (**h**). **i**, Illustration of the incorporation of the tracer ^{15}N from $^{15}NH_4Cl$ into ^{15}N-glutamate in *Got1*-sufficient donor P14 $CD8^+$ T cells. 'm + 0' or 'm + 1' indicates glutamate with zero or one ^{15}N atom. **j**, A bar graph shows amounts of ^{15}N-glutamate. Data are combined from two experiments with eight (**b**–**d**,**f**–**h**) or three (**j**) mice. The data are presented as mean ± s.d. $^*P < 0.05$; $^{**}P < 0.01$; $^{***}P < 0.001$; $^{****}P < 0.0001$. Comparisons were performed with a two-tailed Student's *t* test (**b**,**d**; data points were normally distributed), two-way ANOVA (**c**,**h**,**j**) and one-way ANOVA (**f**,**g**). In **b**, $P = 0.0131$; in **c** (from left to right), $P = 1.4 \times 10^{-14}$, $P = 0.071$, $P = 0.713$, $P = 6.8 \times 10^{-14}$, $P = 0.207$, $P = 0.860$, $P = 0.991$ and $P = 0.671$; in **d**, $P = 1.0 \times 10^{-10}$; in **f** (top), $P = 1.0 \times 10^{-15}$, $P = 0.000403208$, $P = 1.0 \times 10^{-15}$, $P = 1.0 \times 10^{-15}$, $P = 1.0 \times 10^{-15}$, $P = 1.0 \times 10^{-15}$, $P = 1.0 \times 10^{-15}$ and (bottom) $P = 1.0 \times 10^{-15}$, $P = 0.048$, $P = 0.021$, $P = 0.0005$, $P = 1.0 \times 10^{-15}$, $P = 1.0 \times 10^{-15}$, $P = 1.0 \times 10^{-15}$; in **g**, $P = 0.0001$, $P = 1.0 \times 10^{-15}$, $P = 1.0 \times 10^{-15}$, $P = 0.040$, $P = 0.009$, $P = 1.0 \times 10^{-15}$, $P = 1.0 \times 10^{-15}$, $P = 1.0 \times 10^{-15}$ and $P = 1.0 \times 10^{-15}$; in **h**, $P = 0.7694$, $P = 0.373$, $P = 0.0009$ and $P = 5.438 \times 10^{-9}$; in **j**, both $P = 1.2 \times 10^{-5}$. Six-week-old female mice were used (**b**–**h**,**j**). NS, not significant.

Got1 KO $CD8^+$ T cells (Extended Data Fig. 6c,d), suggesting that GOT1 promoted the formation of $CD8^+$ T_{eff} cells in acute infections dependent on the traditional function of GOT1 in maintaining the NAD^+/NADH ratio.

Got1-deficient $CD8^+$ T cells are similar to ammonia-treated WT $CD8^+$ T cells

To compare the effect of *Got1* deficiency versus ammonia treatment on the global transcriptional profiles and epigenetic landscapes, we

performed RNA sequencing and assay for transposase-accessible chromatin (ATAC) sequencing analyses of four groups of $CD8^+$ T cells (Fig. 4a). The pair of *Got1* KO P14 $CD8^+$ T cells and NH_4OH-treated *Got1* WT P14 $CD8^+$ T cells shared the highest degree of similarity with the least differentially expressed genes (Fig. 4b). We further correlated *Got1* deficiency-induced changes in gene expression with those caused by NH_4OH treatment and found that these two groups of differentially expressed genes closely correlated with each other ($R = 0.62$) (Fig. 4c). 686 or 1,049 genes were unanimously increased or decreased, respectively, by *Got1* deficiency and by NH_4OH treatment (Fig. 4d,e).

Both *Got1* deficiency and NH_4OH treatment decreased the expression of genes promoting cell survival and increased the expression of genes promoting cell death (Fig. 4f). *Got1* deficiency and ammonia treatment also decreased the expression levels of the cell proliferation-associated genes, with the exception of *Mki67*, which was decreased by *Got1* deficiency but not ammonia treatment. One possible explanation was that the 8 h ammonia treatment in vitro was not sufficiently long to markedly decrease the expression of *Mki67*. Multiple genes known to be induced by NH_4OH, such as *Nr1d1, Nr1d2, Per2*, *Slc25a3* and *Slc6a6* (refs. 31,32), were also upregulated in *Got1* KO T cells, thereby suggesting that *Got1* deficiency conferred T cells a phenotype resembling that of NH_4OH-treated T cells. Ammonia exposure also inhibited the expression of *Tox*, which is required for maintaining the phenotype and survival of T_{ex} cells[33–36]. Moreover, *Tcf7*, *Il7r*, *Sell* and *Ikzf2*, whose expression is decreased by *Tox* deficiency[33–36], were also inhibited by both *Got1* deficiency and ammonia treatment (Fig. 4f). Similar to the gene expression, global chromatin accessibility was also influenced by *Got1* deficiency and by ammonia treatment, as demonstrated by volcano plots (Fig. 4g), correlation analysis (Fig. 4h) and Venn diagrams comparing the open chromatin regions between the indicated groups of $CD8^+$ T cells (Fig. 4i,j). *Tcf7* and *Bcl2*, whose gene expression levels were unanimously decreased by *Got1* deficiency and ammonia treatment, were also less accessible in *Got1* KO T cells and in ammonia-treated T cells (Fig. 4k). Because 2-KG is involved in multiple biological processes, such as demethylation, the TCA cycle and HIF proteins, we conducted further analysis to examine whether *Got1* deficiency and ammonia treatment influenced the expression levels of genes involved in these biological processes (Extended Data Fig. 7). We found that both *Got1* deficiency and ammonia treatment decreased the expression levels of genes involved in demethylation, such as *Kdm6b* and *Tet1*. Conversely, the expression levels of *Tet3* were increased in *Got1*-deficient cells and ammonia-treated cells. This increase in *Tet3* expression may represent a compensatory mechanism to counterbalance the reduced expression of *Kdm6b* and *Tet1*. Furthermore, the expression levels of genes encoding TCA enzymes were generally decreased by *Got1* deficiency and ammonia treatment. Additionally, we found that *Got1* deficiency and ammonia treatment reduced the mRNA levels of *Hif1a* and *Hif3a* and increased the expression of *Epas*1 (encoding the HIF2a protein). Together, these results suggested that *Got1* deficiency influenced the transcriptional profiles and epigenetic landscapes of $CD8^+$ T cells in a manner similar to ammonia treatment.

GOT1 catalyzes an atypical chemical reaction in $CD8^+$ T_{ex} cells

To monitor electron transport in $CD8^+$ T cells (Fig. 5a), we performed mitochondrial electron flow analysis of $CD8^+$ T_{ex} cells and $CD8^+$ T_{mem} cells by using a Seahorse extracellular flux analyzer (Fig. 5b–d). We pretreated $CD8^+$ T_{ex} cells and $CD8^+$ T_{mem} cells with plasma membrane permeabilizer (PMP), which permeabilizes plasma membranes but not mitochondrial membranes. Therefore, PMP treatment enables the monitoring of mitochondrial metabolism without the need for purifying mitochondria. The oxygen consumption rate (OCR) in $CD8^+$ T_{mem} cells responded robustly to rotenone (an inhibitor of mitochondrial complex I), succinate (a substrate for mitochondrial complex II), antimycin A (an inhibitor of mitochondrial complex III), and ascorbate (Asc) and N,N,N′,N′-tetramethyl-para-phenylene-diamine (TMPD) (substrates for mitochondrial complex IV), suggesting that $CD8^+$ T_{mem} cells underwent active electron transportation through the mitochondrial complex to oxygen. By contrast, the OCR was much lower in $CD8^+$ T_{ex} cells, and $CD8^+$ T_{ex} cells responded poorly to inhibitors and substrates of mitochondrial complexes (Fig. 5b). The OCR of $CD8^+$ T_{ex} cells resembled that of $CD8^+$ T_{mem} cells treated with antimycin A and azide (inhibitors of mitochondrial complex III and IV) or NH_4OH, respectively (Fig. 5c,d). Collectively, these results suggested that electron transport through ETC of $CD8^+$ T_{ex} cells was inhibited with respect to that in $CD8^+$ T_{mem} cells.

GOT1 catalyzes an atypical chemical reaction that generates 2-KG and aspartate from oxaloacetate and glutamate in human Jurkat leukemic T cells when respiration is inhibited[37]. We examined whether GOT1 also catalyzed this atypical chemical reaction in $CD8^+$ T_{ex} cells (Fig. 5e). We pulsed $CD8^+$ T_{ex} cells with ^{13}C tracer-labeled malate. In the conventional malate shuttle, GOT2, but not GOT1, is required to generate 2-KG and aspartate. *Got1* deficiency was not expected to affect the incorporation of ^{13}C tracer into aspartate. If GOT1 catalyzed the atypical chemical reaction, as previously reported[37], the incorporation of the ^{13}C tracer into aspartate would be affected by *Got1* deficiency. *Got1* WT and *Got1* KO $CD8^+$ T_{mem} cells generated comparable amounts of ^{13}C tracer-labeled aspartate (Fig. 5f), thus suggesting that $CD8^+$ T_{mem} cells underwent the conventional malate shuttle chemical reactions and did not require GOT1 to generate aspartate. By contrast, *Got1* KO $CD8^+$ T_{ex} cells generated less ^{13}C tracer-labeled aspartate than *Got1* WT $CD8^+$ T_{ex} cells (Fig. 5f), suggesting that $CD8^+$ T_{ex} cells required GOT1 to generate aspartate from malate. Collectively, these results suggested that GOT1 catalyzes an atypical chemical reaction in $CD8^+$ T_{ex} cells with respiratory inhibition.

$CD8^+$ T_{ex} cells require GOT1 to catabolize glutamate

Ammonia is produced by the deamination of glutamine and glutamate (Fig. 5g). The initial step of glutaminolysis is the conversion of glutamine to glutamate and ammonia. After this initial step, two different chemical pathways catabolize glutamate. First, glutamate dehydrogenase (GDH)-1 converts glutamate to 2-KG and ammonia. Second, glutamate is converted to 2-KG by GOT1 through atypical chemical reactions, as illustrated above (Fig. 5e), or by GOT2 through the conventional malate shuttle. Because the ammonia scavenger

Fig. 4 | *Got1*-deficient $CD8^+$ T cells are similar to ammonia-treated *Got1*-sufficient $CD8^+$ T cells. a, Experimental design. *Got1*-deficient and sufficient donor P14 $CD8^+$ T cells were isolated from C57BL/6 host mice infected with LCMV clone 13 8 d earlier. *Got1*-deficient P14 cells and one fraction of *Got1*-sufficient P14 cells were directly used for RNA-sequencing analysis and ATAC-sequencing analysis. The other fractions of *Got1*-sufficient P14 cells were cultured with anti-CD3 and anti-CD28 in the presence or absence of 1 mM ammonium hydroxide for 8 h before RNA-sequencing analysis and ATAC-sequencing analysis. **b**,**g**, Volcano plots show the differentially expressed genes (**b**) or differentially accessible peaks (**g**). **c**,**h**, Dot plots show the correlation between *Got1* deficiency-induced changes in gene expression and ammonia treatment-induced changes in gene expression (**c**) or the correlation between *Got1* deficiency-induced changes in chromatic openness and ammonia treatment-induced changes in chromatic openness (**h**) in the indicated groups of cells. **d**,**e**,**i**,**j**, Venn diagrams show the numbers of genes (**d**,**e**) or accessible peaks (**i**,**j**) overlapping between the indicated groups of comparisons. **f**, Heat map shows the mRNA expression *z* scores of the indicated genes in the four groups of cells. **k**, ATAC-sequencing signal profiles across *Tcf7* and *Bcl2* loci in the indicated groups of P14 $CD8^+$ T cells. $n = 3$ mice in each of the four groups (**b**–**k**). Comparisons were performed with a two-sided Wald test, and *P* values were adjusted with the Benjamini–Hochberg procedure (**b**,**g**) or a two-tailed Student's *t* test (**c**,**h**). Six-week-old male mice were used (**b**–**k**). FC, fold change.

https://doi.org/10.1038/s41590-023-01636-5

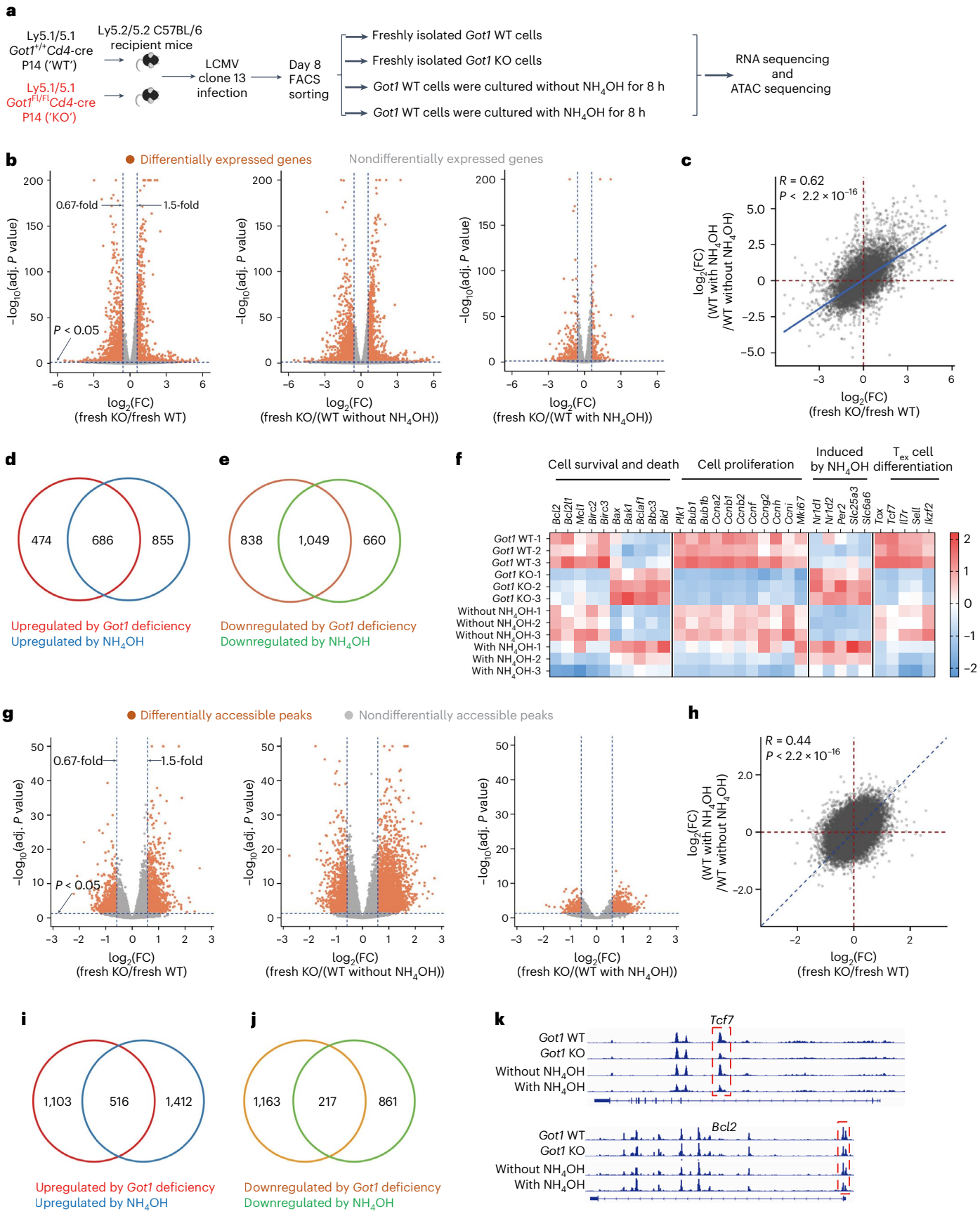

https://doi.org/10.1038/s41590-023-01636-5

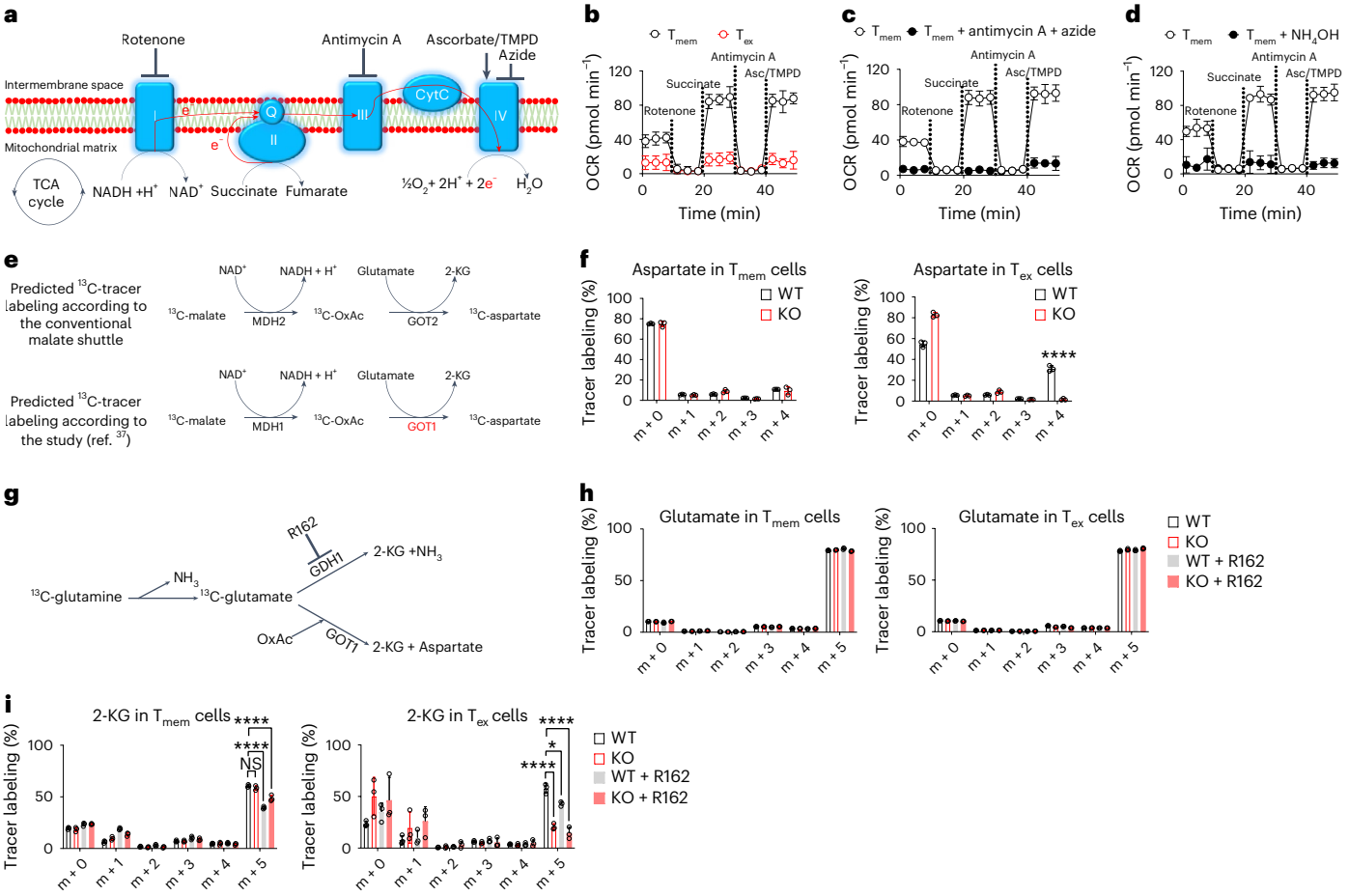

Fig. 5 | T_{ex} cells require GOT1 to produce 2-KG by an 'ammonia-neutral pathway'. a, Electron flow through mitochondrial complexes. **b**–**d**, WT donor P14 $CD8^+$ T cells were isolated from C57BL/6 host mice that were infected with LCMV clone 13 or LCMV Armstrong 30 d earlier. T_{ex} or T_{mem} donor P14 $CD8^+$ cells were FACS-purified and permeabilized with PMP. Mitochondrial complex inhibitors (rotenone and antimycin A inhibit complexes I and III, respectively) and substrates (succinate, a substrate for complex II; Asc and TMPD, substrates for complex IV) were supplemented sequentially into the T cell culture as indicated. Line graphs show the OCR values of PMP-permeabilized T_{ex} cell versus T_{mem} cells (**b**), T_{mem} cell versus T_{mem} cells treated with antimycin A and azide (**c**), or T_{mem} cell versus T_{mem} cells treated with NH_4OH (**d**) in Seahorse electron flow assays. **e**, Illustration of the incorporation of the tracer ^{13}C from ^{13}C-malate into ^{13}C-aspartate. **f**, Bar graphs show amounts of ^{13}C-aspartate in T_{mem} cells and T_{ex} cells. 'm + 4' indicates aspartate with four ^{13}C atoms. **g**, Illustration of the incorporation of the tracer ^{13}C from ^{13}C-glutamine into ^{13}C-glutamate or ^{13}C-2-KG. **h**,**i**, Bar graphs show amounts of ^{13}C-glutamate (**h**) or ^{13}C-2-KG (**i**) in T_{mem} cells and T_{ex} cells. 'm + 5' indicates glutamate (**h**) or 2-KG (**i**) with five ^{13}C atoms. Data are combined from two experiments with six mice (**b**–**d**), 15 host mice containing *Got1*-sufficient donor P14 $CD8^+$ T cells, and 30 host mice containing *Got1*-deficient donor P14 $CD8^+$ T cells (**f**,**h**,**i**). Data are mean ± s.d. $^*P < 0.05$; $^{****}P < 0.0001$. Comparisons were performed with two-way ANOVA (**f**,**h**,**i**). In **f**, $P = 2.0 \times 10^{-15}$; in **i**, $P = 0.066993749$, $P < 1.0 \times 10^{-15}$, $P = 1.0 \times 10^{-14}$, $P = 6.7 \times 10^{-7}$, $P = 0.025248392$ and $P = 2.2 \times 10^{-8}$. Six-week-old female mice were used (**b**–**d**,**f**,**h**,**i**).

2-KG is generated without the production of free ammonia in the second pathway, we refer to this pathway as the 'ammonia-neutral pathway'.

To test whether *Got1* deficiency influenced the production of free ammonia, we measured the rates of glutaminolysis by pulsing *Got1* WT or *Got1* KO $CD8^+$ T_{ex} cells and $CD8^+$ T_{mem} cells with ^{13}C tracer-labeled glutamine. During the period of observation, *Got1* WT and *Got1* KO $CD8^+$ T cells generated comparable amounts of ^{13}C tracer-labeled glutamate from glutamine (Fig. 5h). These results suggested that *Got1* deficiency did not influence the initial deamination step of glutaminolysis, at least in the short term.

To examine the individual contributions of the GOT1-dependent ammonia-neutral pathway and GDH1-dependent ammonia-generating pathway in glutamine catabolism, we pulsed *Got1* WT and KO $CD8^+$ T cells with ^{13}C tracer-labeled glutamine in the presence or absence of GDH1 inhibitor R162 (Fig. 5g). Inhibiting GDH1 by R162 decreased the incorporation of ^{13}C tracers into 2-KG in $CD8^+$ T_{mem} cells, but the amounts of ^{13}C tracers in 2-KG were comparable between *Got1* WT and KO $CD8^+$ T_{mem} cells (Fig. 5i). These results suggested that glutamate relied on the GDH1-mediated pathway to generate 2-KG in $CD8^+$ T_{mem} cells. By contrast, *Got1* deficiency decreased 2-KG production from glutamate in $CD8^+$ T_{ex} cells. Furthermore, *Got1* deficiency combined with GDH1 inhibition almost completely blocked the conversion from glutamate to 2-KG (Fig. 5i). These results suggested that $CD8^+$ T_{mem} cells and T_{ex} cells underwent the initial deamination step of glutaminolysis at comparable rates. At the second step, however, $CD8^+$ T_{ex} cells had a greater reliance on the GOT1-mediated ammonia scavenger-generating pathway than $CD8^+$ T_{mem} cells, which underwent GDH1-dependent deamination.

2-KG restores *Got1*-deficient $CD8^+$ T cell-mediated antiviral responses

To test whether 2-KG enhanced *Got1* KO $CD8^+$ T cell-mediated antiviral responses in vivo, we adoptively transferred *Got1* KO and WT P14 $CD8^+$ T cells into C57BL/6 mice and infected these mice with LCMV clone 13. We treated these mice with 2-KG or vehicle control (Fig. 6a). The total

https://doi.org/10.1038/s41590-023-01636-5

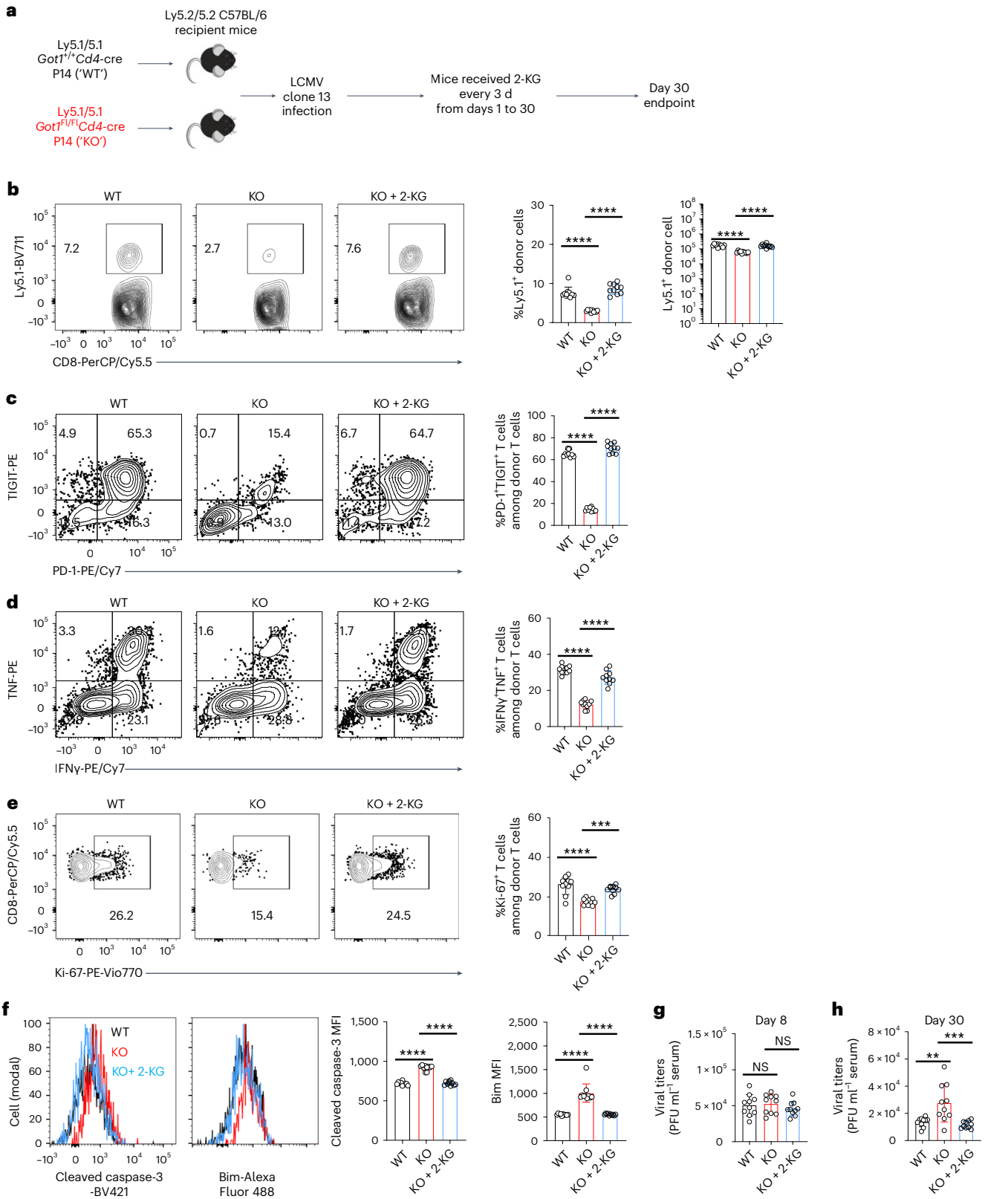

Fig. 6 | 2-KG restores *Got1*-deficient CD8⁺ T cell antiviral responses in vivo. **a**, Experimental design. **b**–**f**, Contour plots, histograms and bar graphs show the flow cytometry staining results of Ly5.1⁺ donor P14 CD8⁺ T cells (**b**), PD-1 and TIGIT (**c**), cytokines (**d**), Ki-67 (**e**), and cleaved caspase-3 and Bim (**f**) in *Got1*-deficient and sufficient P14 CD8⁺ T cells. Cells were stimulated with $GP_{33–41}$ peptides before flow cytometry staining (**d**). **g**,**h**, Bar graphs show the viral titers at day 8 (**g**) and day 30 (**h**) after infections. Data were pooled from two independent experiments (**b**–**h**). $n = 10$ C57BL/6 mice per group. The results are presented as mean ± s.d. $^{**}P < 0.01$; $^{***}P < 0.001$; $^{****}P < 0.0001$. Comparisons were performed with one-way ANOVA. In **b**, $P = 1.6 \times 10^{-9}$, $P = 3.2 \times 10^{-11}$, $P = 1.3 \times 10^{-7}$ and $P = 5.8 \times 10^{-7}$; in **c**, both $P = 1.1 \times 10^{-14}$; in **d**, $P = 4.5 \times 10^{-14}$ and $P = 1.1 \times 10^{-11}$; in **e**, $P = 2.5 \times 10^{-6}$ and $P = 0.00015972$; in **f**, $P = 1.7 \times 10^{-14}$, $P = 1.9 \times 10^{-14}$, $P = 3.7 \times 10^{-9}$ and $P = 4.0 \times 10^{-9}$; in **g**, $P = 0.937$ and $P = 0.477$; in **h**, $P = 0.002629596$ and $P = 0.000658958$. Six-week-old female mice were used (**b**–**h**).

https://doi.org/10.1038/s41590-023-01636-5

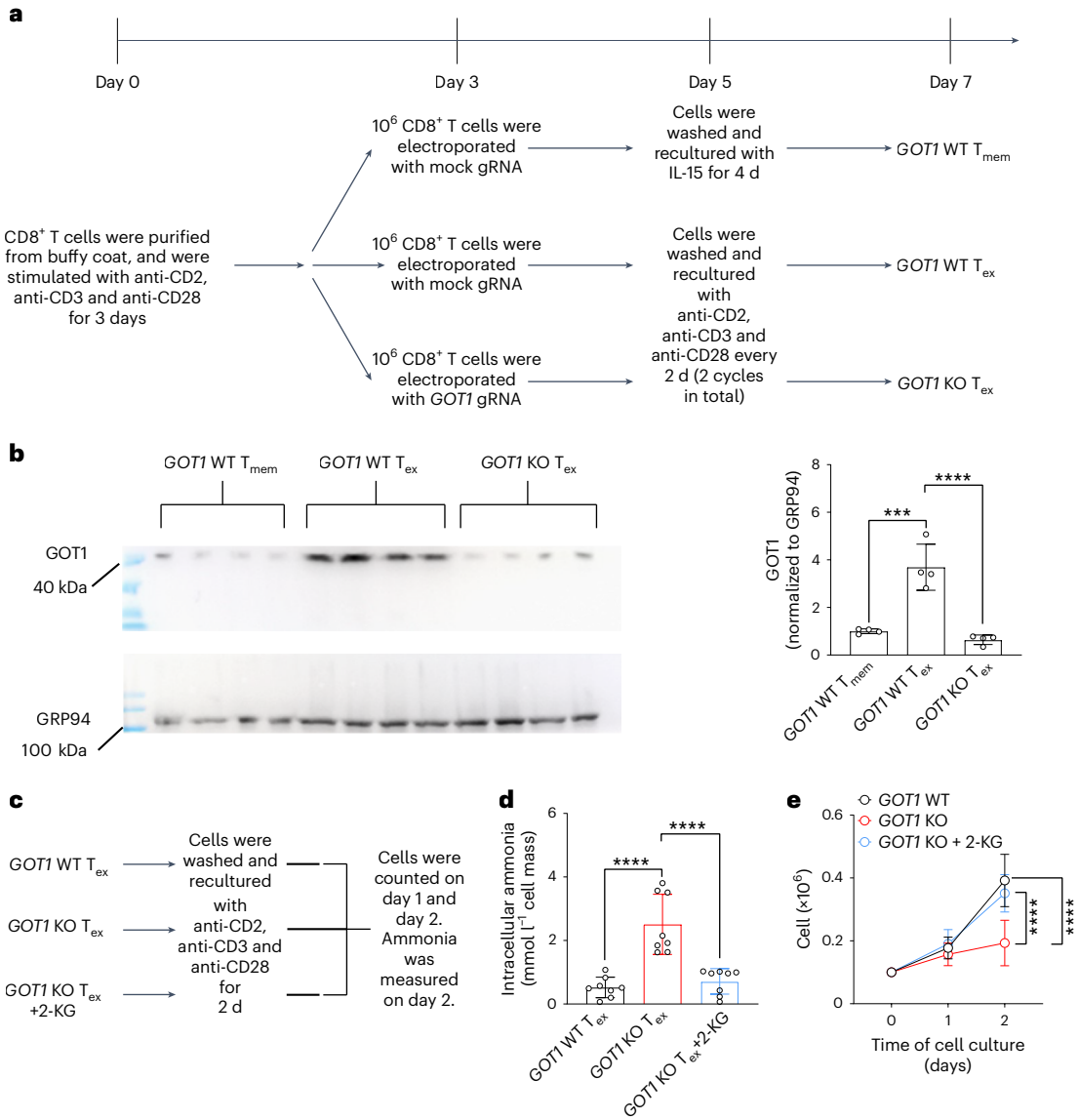

Fig. 7 | 2-KG decreases ammonia and restores survival of *GOT1*-deficient human CD8⁺ T cells. a, Experimental design of **b**. Healthy donor CD8⁺ T cells were electroporated with Cas9 protein and *GOT1*-specific gRNA and were differentiated into T_{ex}-like cells or T_{mem}-like cells. **b**, Western blot images show the expression of GOT1 in the indicated populations of cells. GRP94 was used as a loading control. A bar graph shows the results of densitometric quantification of the GOT1 immunoblot bands. **c**, Illustration of the experimental design of **d** and **e**. **d**, Bar graph shows the concentrations of ammonia in CD8⁺ T cells. **e**, A line graph shows the numbers of cells on day 1 and day 2 after restimulation with anti-CD2, anti-CD3 and anti-CD28. Data are cumulative from two independent experiments with eight healthy donors in total. Results are mean ± s.d. ***$P < 0.001$; ****$P < 0.0001$. Comparisons were performed with one-way ANOVA (**b**,**d**) or two-way ANOVA (**e**). In **b**, $P = 0.000192726$ and $P < 1.0 \times 10^{-15}$; in **d**, both $P < 1.0 \times 10^{-15}$; in **e** (from top to bottom), $P = 6.4 \times 10^{-11}$ and $P = 6.7 \times 10^{-8}$.

numbers of *Got1* KO donor T cells significantly increased after 2-KG treatment to a level comparable to that observed in *Got1* WT donor T cells (Fig. 6b). In addition, 2-KG significantly increased PD-1 expression (Fig. 6c) and promoted IFNγ and TNF production in *Got1* KO donor T cells (Fig. 6d). Furthermore, 2-KG restored the expression of Ki-67 (Fig. 6e) and decreased the expression levels of apoptosis-associated cleaved caspase-3 and Bim in *Got1* KO donor T cells (Fig. 6f). Viral titers were comparable between the '*Got1* WT' group and the '*Got1* KO' group on day 8 after LCMV clone 13 infections (Fig. 6g). However, on day 30, C57BL/6 mice that received *Got1* KO P14 CD8⁺ T cells exhibited higher viral titers than those receiving *Got1* WT P14 CD8⁺ T cells. Treatment with 2-KG reduced the viral titers in the serum of C57BL/6 mice that received *Got1* KO P14 CD8⁺ T cells (Fig. 6h). These results suggest that *Got1* deficiency affected antiviral CD8⁺ T cell responses, which was restored by 2-KG treatment.

2-KG decreases ammonia and restores survival of *GOT1*-deficient human CD8⁺ T cells

To examine the expression levels of GOT1 protein in human T_{ex} cells and T_{mem} cells, we followed a previously published protocol[38] to generate T_{ex} cells and T_{mem} cells in vitro (Fig. 7a). T_{ex} cells expressed higher levels of GOT1 protein than T_{mem} cells (Fig. 7b). We used CRISPR/Cas9 technology to generate human *GOT1*-deficient CD8⁺ T cells, which expressed low levels of GOT1 protein (Fig. 7b). To examine whether *GOT1* deficiency increased ammonia accumulation in T_{ex} cells and caused *GOT1* KO CD8⁺ T cell death, we treated *GOT1* KO T_{ex} cells with 2-KG (Fig. 7c). *GOT1* KO T_{ex} cells produced higher levels of ammonia than *GOT1* WT T_{ex} cells, and 2-KG decreased the ammonia in *GOT1* KO T_{ex} cells to a level comparable to that in *GOT1* WT T_{ex} cells (Fig. 7d). Furthermore, 2-KG restored *GOT1* KO T_{ex} cell survival (Fig. 7e), in line with our mouse model results showing that 2-KG increased the numbers of T_{ex} cells during LCMV

clone 13 chronic infection (Fig. 6b). Collectively, these results suggested that human T_{ex} cells relied on GOT1 to detoxify ammonia.

We discovered that $CD8^+$ T_{ex} cells expressed high levels of GOT1 during chronic viral infection. GOT1 promoted the survival of human and mouse $CD8^+$ T_{ex} cells by catalyzing an unconventional chemical reaction producing 2-KG. 2-KG assimilated ammonia and enabled sustainable ammonia-neutral glutaminolysis in $CD8^+$ T_{ex} cells. Our work sheds new light on the plasticity of GOT1-catalyzed chemical reaction networks and reveals that T_{ex} cells rewire the malate shuttle-associated metabolic pathways when respiration is inhibited.

The longitudinal expression kinetics of GOT1 resembled that of the inhibitory receptors PD-1 and TIGIT, which were transiently expressed during acute infection and persistently expressed during chronic infection. *Got1* deficiency shrank the pool of $CD8^+$ T cells expressing PD-1 and TIGIT but did not affect the homeostasis of naïve $CD8^+$ T cells, suggesting that GOT1 was selectively required for the survival of PD-1^+TIGIT$^+$ $CD8^+$ T cells. This finding is reminiscent of the requirement of TOX for maintaining the survival of $CD8^+$ T_{ex} cells but not naïve T cells[33–36]. The selective expression of GOT1 in T_{ex} cells presents an opportunity to regulate the metabolism and survival of T_{ex} cells through pharmacological or genetic approaches.

Environmental ammonia's toxicity has been extensively studied[39,40]. In contrast to environmental ammonia, whose exposure is rare, endogenous ammonia is constantly produced from amino acid metabolism and should be detoxified through continuously active mechanisms. The urea cycle is active in the liver and detoxifies ammonia by converting ammonia into urea, which is removed through excretion[41]. A recent study has suggested that the urea cycle is also active in T cells[42]. The current study suggested that the GOT1-mediated production of 2-KG assimilated ammonia and protected $CD8^+$ T cells against high concentrations of free ammonia-induced cell death. This GOT1-mediated mechanism complements the urea cycle, thereby preventing the in situ accumulation of ammonia in T cells, and allowing antiviral T cells to undergo glutamine catabolism in a sustainable manner.

Our data revealed that GOT1 catalyzes an unconventional chemical reaction in $CD8^+$ T_{ex} cells. This observation confirms previous reports showing that GOT1 is required to convert oxaloacetate and glutamate into aspartic acid and 2-KG when the respiratory chain is inhibited[37]. *Got1*-deficient and *Got1*-sufficient $CD8^+$ T_{ex} cells had comparable levels of aspartic acid. One possible explanation is that the aspartic acid transporter in *Got1*-deficient $CD8^+$ T_{ex} cells imported exogenous aspartic acid and compensated for the decreased synthesis of aspartic acid. The comparable levels of aspartic acid between *Got1*-deficient and *Got1*-sufficient T_{ex} cells also suggested that synthesizing aspartic acid was not the only driving force in GOT1's catalysis of the unconventional chemical reaction. Ammonia accumulation also contributed to reversing the conventional chemical reaction to produce the ammonia scavenger 2-KG.

Overall, our findings revealed that GOT1 is induced by persistent TCR stimulation during chronic infection. GOT1 catalyzes an unconventional chemical reaction in $CD8^+$ T_{ex} cells under respiratory inhibition, thereby producing the ammonia scavenger 2-KG, which detoxifies ammonia and is required for $CD8^+$ T_{ex} cell survival. This study suggests that $CD8^+$ T_{ex} cells adapt to persistent extracellular antigen stimulation by rewiring glutamine catabolism from the ammonia-producing pathway to the ammonia-neutral pathway, which promote $CD8^+$ T_{ex} cell metabolic fitness.

Online content

Any methods, additional references, Nature Portfolio reporting summaries, source data, extended data, supplementary information, acknowledgements, peer review information; details of author contributions and competing interests; and statements of data and code availability are available at https://doi.org/10.1038/s41590-023-01636-5.

References

1. McLane, L. M., Abdel-Hakeem, M. S. & Wherry, E. J. CD8 T cell exhaustion during chronic viral infection and cancer. *Annu. Rev. Immunol.* **37**, 457–495 (2015).
2. Bengsch, B. et al. Bioenergetic insufficiencies due to metabolic alterations regulated by the inhibitory receptor PD-1 are an early driver of $CD8^+$ T cell exhaustion. *Immunity* **45**, 358–373 (2016).
3. Staron, M. M. et al. The transcription factor FoxO1 sustains expression of the inhibitory receptor PD-1 and survival of antiviral $CD8^+$ T cells during chronic infection. *Immunity* **41**, 802–814 (2014).
4. Berg, J. M. *Biochemistry* (W H Freeman, 2007).
5. Wang, R. et al. The transcription factor Myc controls metabolic reprogramming upon T lymphocyte activation. *Immunity* **35**, 871–882 (2011).
6. Beeler, T. & Churchich, J. E. Reactivity of the phosphopyridoxal groups of cystathionase. *J. Biol. Chem.* **251**, 5267–5271 (1976).
7. Löscher, W. Effect of inhibitors of GABA transaminase on the synthesis, binding, uptake and metabolism of GABA. *J. Neurochem.* **34**, 1603–1608 (1980).
8. Braunstein, A. E., Goryachenkova, E. V., Tolosa, E. A., Willhardt, I. H. & Yefremova, L. L. Specificity and some other properties of liver serine sulphhydrase: evidence for its identity with cystathionine β-synthase. *Biochim. Biophys. Acta* **242**, 247–260 (1971).
9. Wherry, E. J. et al. Molecular signature of $CD8^+$ T cell exhaustion during chronic viral infection. *Immunity* **27**, 670–684 (2007).
10. Shin, H., Blackburn, S. D., Blattman, J. N. & Wherry, E. J. Viral antigen and extensive division maintain virus-specific CD8 T cells during chronic infection. *J. Exp. Med.* **204**, 941–949 (2007).
11. Prevost-Blondel, A. et al. Tumor-infiltrating lymphocytes exhibiting high ex vivo cytolytic activity fail to prevent murine melanoma tumor growth in vivo. *J. Immunol.* **161**, 2187–2194 (1998).
12. Rooney, J. W., Sun, Y. L., Glimcher, L. H. & Hoey, T. Novel NFAT sites that mediate activation of the interleukin-2 promoter in response to T-cell receptor stimulation. *Mol. Cell. Biol.* **15**, 6299–6310 (1995).
13. Seo, H. et al. TOX and TOX2 transcription factors cooperate with NR4A transcription factors to impose $CD8^+$ T cell exhaustion. *Proc. Natl Acad. Sci. USA* **116**, 12410–12415 (2019).
14. Intlekofer, A. M. et al. Effector and memory $CD8^+$ T cell fate coupled by T-bet and eomesodermin. *Nat. Immunol.* **6**, 1236–1244 (2005).
15. Ji, Y. et al. Repression of the DNA-binding inhibitor Id3 by Blimp-1 limits the formation of memory $CD8^+$ T cells. *Nat. Immunol.* **12**, 1230–1237 (2011).
16. Philip, M. et al. Chromatin states define tumour-specific T cell dysfunction and reprogramming. *Nature* **545**, 452–456 (2017).
17. Pauken, K. E. et al. Epigenetic stability of exhausted T cells limits durability of reinvigoration by PD-1 blockade. *Science* **354**, 1160–1165 (2016).
18. Lee, P. P. et al. A critical role for Dnmt1 and DNA methylation in T cell development, function, and survival. *Immunity* **15**, 763–774 (2001).
19. Sawada, S., Scarborough, J. D., Killeen, N. & Littman, D. R. A lineage-specific transcriptional silencer regulates *CD4* gene expression during T lymphocyte development. *Cell* **77**, 917–929 (1994).
20. Dahlbender, B. & Strack, D. The role of malate in ammonia assimilation in cotyledons of radish (*Raphanus sativus L.*). *Planta* **169**, 382–392 (1986).
21. Loginova, N. V., Govorukhina, N. I. & Trotsenko Iu, A. Enzymes of ammonia assimilation in bacteria with different C1-metabolic pathways. *Mikrobiologiia* **51**, 38–42 (1982).

22. Koizumi, T., Hayakawa, J. & Nikaido, H. Blood ammonia concentration in mice: normal reference values and changes during growth. *Lab. Anim. Sci.* **40**, 308–311 (1990).
23. Heeneman, S., Deutz, N. E. P. & Buurman, W. A. The concentrations of glutamine and ammonia in commercially available cell culture media. *J. Immunol. Methods* **166**, 85–91 (1993).
24. Carey, B. W., Finley, L. W., Cross, J. R., Allis, C. D. & Thompson, C. B. Intracellular α-ketoglutarate maintains the pluripotency of embryonic stem cells. *Nature* **518**, 413–416 (2015).
25. Tsukada, Y.-I. et al. Histone demethylation by a family of JmjC domain-containing proteins. *Nature* **439**, 811–816 (2006).
26. Tahiliani, M. et al. Conversion of 5-methylcytosine to 5-hydroxymethylcytosine in mammalian DNA by MLL partner TET1. *Science* **324**, 930–935 (2009).
27. Ito, S. et al. Role of Tet proteins in 5mC to 5hmC conversion, ES-cell self-renewal and inner cell mass specification. *Nature* **466**, 1129–1133 (2010).
28. Kruidenier, L. et al. A selective jumonji H3K27 demethylase inhibitor modulates the proinflammatory macrophage response. *Nature* **488**, 404–408 (2012).
29. Xu, W. et al. Oncometabolite 2-hydroxyglutarate Is a competitive inhibitor of α-ketoglutarate-dependent dioxygenases. *Cancer Cell* **19**, 17–30 (2011).
30. Chowdhury, R. et al. The oncometabolite 2-hydroxyglutarate inhibits histone lysine demethylases. *EMBO Rep.* **12**, 463–469 (2011).
31. Wang, X. et al. Ammonia exposure causes lung injuries and disturbs pulmonary circadian clock gene network in a pig study. *Ecotoxicol. Environ. Saf.* **205**, 111050 (2020).
32. Xia, C., Zhang, X., Zhang, Y., Li, J. & Xing, H. Ammonia exposure causes the disruption of the solute carrier family gene network in pigs. *Ecotoxicol. Environ. Saf.* **210**, 111870 (2021).
33. Alfei, F. et al. TOX reinforces the phenotype and longevity of exhausted T cells in chronic viral infection. *Nature* **571**, 265–269 (2019).
34. Scott, A. C. et al. TOX is a critical regulator of tumour-specific T cell differentiation. *Nature* **571**, 270–274 (2019).
35. Khan, O. et al. TOX transcriptionally and epigenetically programs $CD8^+$ T cell exhaustion. *Nature* **571**, 211–218 (2019).
36. Yao, C. et al. Single-cell RNA-seq reveals TOX as a key regulator of $CD8^+$ T cell persistence in chronic infection. *Nat. Immunol.* **20**, 890–901 (2019).
37. Birsoy, K. et al. An essential role of the mitochondrial electron transport chain in cell proliferation is to enable aspartate synthesis. *Cell* **162**, 540–551 (2015).
38. Zhao, M. et al. Rapid in vitro generation of bona fide exhausted $CD8^+$ T cells is accompanied by Tcf7 promotor methylation. *PLoS Pathog.* **16**, e1008555 (2020).
39. Dasarathy, S. et al. Ammonia toxicity: from head to toe? *Metab. Brain Dis.* **32**, 529–538 (2017).
40. Shah, S. W. A. et al. The effect of ammonia exposure on energy metabolism and mitochondrial dynamic proteins in chicken thymus: through oxidative stress, apoptosis, and autophagy. *Ecotoxicol. Environ. Saf.* **206**, 111413 (2020).
41. Jackson, M. J., Beaudet, A. L. & O'Brien, W. E. Mammalian urea cycle enzymes. *Annu. Rev. Genet* **20**, 431–464 (1986).
42. Tang, K. et al. Ammonia detoxification promotes $CD8^+$ T cell memory development by urea and citrulline cycles. *Nature Immunol.* **24**, 162–173 (2023).

Methods

Mice

Mice were maintained in the German Cancer Research Center (DKFZ), a specific pathogen-free facility. All studies were performed in accordance with DKFZ regulations with approval by the German regional council at the Regierungspräsidium Karlsruhe (G-232/16). The *Got1*$^{Flox/Flox}$ mice, under the full name C57BL/6N-$^{Got1tm1c(EUCOMM)Hmgu}$/H, were ordered from the MRC Harwell Institute, Oxfordshire, UK. Exon 2 of *Got1* is flanked by two LoxP sites and is excised after crossing with a Cre-expression mouse strain. *Cd4*-Cre mice[18,19] and P14 mice[43] were from The Jackson Laboratory and have been backcrossed to C57BL/6N background for more than ten generations. Mice were housed with a 12-h day/12-h night cycle in a controlled environment at 20–24 °C and 45–65% humidity and were fed a regular chow diet (Kliba Nafag, 3437) ad libitum. We used sex-matched and age-matched (6–7-week-old) mice for each individual experiment. In rare cases, mice with fighting wounds were excluded from the experimental analysis. The sample collection and processing were not performed in a blinded manner.

Human samples

For immunofluorescence analysis, HIV patient tissue sections were provided by the tissue bank of the German Center for Infection Research (DZIF) in accordance with the regulations of the tissue bank and the approval of the ethics committee of Heidelberg University. HIV-positive samples were from two male donors (59-year-old and 62-year-old) and 1 female donor (34-year-old). HIV-negative samples were also from 2 male donors (65-year-old and 74-year-old) and 1 female donor (51-year-old). Buffy coat human peripheral blood mononuclear cell (PBMC) samples from healthy donors were provided by the blood bank of Mannheim. There were eight healthy donors in total (24-year-old female, 26-year-old female, 26-year-old male, 40-year-old female, 69-year-old male, 64-year-old male, 58-year-old female and 40-year-old male). Both the immunofluorescence evaluation of human tissue sections and the flow cytometry analysis of T cells from healthy donor PBMCs were conducted in accordance with the Declaration of Helsinki. Written informed consent was obtained from the patients before the analysis. No compensation was offered.

Human T cell Cas9 and guide RNA electroporation

Healthy donor CD8$^+$ T cells were purified from PBMCs with a CD8$^+$ T cell isolation kit (Miltenyi, 130-096-495) and were pre-activated with anti-CD2, anti-CD3 and anti-CD28 for 3 d before electroporation. We used the predesigned Alt-R CRISPR–Cas9 *GOT1*-specfic CRISPR RNA (crRNA) from Integrated DNA Technologies (design Hs.Cas9.GOT1.1.AA, target sequence ACATTCGGTCCTATCGCTACTGG; design Hs.Cas9.GOT1.1.AB, target sequence ACCTCGGCAAAGACTGACGGAGG and design Hs.Cas9.GOT1.1.AC, target sequence ACGAGTATCTGC CAATCCTGGG). crRNA was annealed with *trans*-activating CRISPR RNA (tracrRNA; Integrated DNA Technologies, 1072534) to form gRNA. We electroporated human CD8$^+$ T cells with Cas9 protein and gRNA according to a previously published protocol[44]. Briefly, 9 µl *GOT1*-specfic gRNA (3 µl design Hs.Cas9.GOT1.1.AA, 3 µl design Hs.Cas9.GOT1.1.AB and 3 µl design Hs.Cas9.GOT1.1.AC, 50 µM stock for each gRNA) and 6 µl Cas9 protein (5 µg ml^{-1} stock, Invitrogen; A36499) were incubated at room temperature for 10 min. tracrRNA was mixed with Cas9 protein as a negative control. A total of 10^7 CD8$^+$ T cells were resuspended in 100 µl P2 solution (Lonza, V4XP-2032) and gently mixed with the RNA–Cas9 protein complexes. The mixture was transferred to a nucleofection cuvette and electroporated with a 4D nucleofector (Lonza, core unit AAF-1002B, X unit AAF-1002X) with the EH100 electroporation program. Electroporated T cells were cultured in IL-7 (Miltenyi, 130-095-361) and allowed to recover overnight. Then T cells were repeatedly stimulated with anti-CD2, anti-CD3 and anti-CD28 for 4 d to differentiate T cells into T_{ex}-like T cells. Another fraction of cells was washed and cultured with IL-15 (Miltenyi, 130-095-762) for 4 d to differentiate into T_{mem}-like T cells.

LCMV infection

C57BL/6 mice were intravenously injected with 5,000 (for subsequent LCMV Armstrong infection) or 500 (for subsequent LCMV clone 13 infection) *Got1*-deficient or -sufficient P14 TCR-transgenic CD8$^+$ cells. These C57BL/6 mice containing P14 CD8$^+$ T cells were infected with LCMV Armstrong (intraperitoneal injection, 2×10^5 plaque-forming units (PFU) per mouse) or LCMV clone 13 (intravenous injection, 2×10^6 PFU per mouse). These mice were killed at the indicated time points (day 8 or day 30 as specified in the figure legends). Spleens were collected for flow cytometry analysis.

B16 melanoma cell implantation

B16 melanoma cells were maintained in DMEM supplemented with 10% FBS, penicillin and streptomycin. To maintain the expression of $GP_{33–41}$ and OVA, we used G418 and blasticidin to supplement the B16-$GP_{33–41}$ and B16-OVA melanoma cell cultures, respectively. B16-$GP_{33–41}$ cells were provided by H. Pircher at the Max Planck Institute of Immunobiology and Epigenetics. B16 and B16-OVA cell lines were provided by R. Carretero in the DKFZ-Bayer Immunotherapeutic Lab. Before tumor cell implantation, we shaved the mice and subcutaneously injected B16 melanoma cells (2×10^5 cells per mouse) into the flanks. We measured tumor sizes every 2–3 d with calipers.

Mouse primary T cell culture

We cultured mouse splenocytes or purified T cells in a complete RPMI 1640 medium supplemented with 10% FBS, HEPES, 2-mercaptoethanol and nonessential amino acids. To culture P14 cells for measuring GOT1 protein levels by western blotting, we cultured *Got1*-deficient or -sufficient P14 splenocytes (1×10^6 ml^{-1} complete medium per well in a 24-well plate) with the cognate $GP_{33–41}$ peptide (10 ng ml^{-1}; GenScript, RP20257) and IL-2 (10 ng ml^{-1}; BioLegend, 575408) for the indicated times. NR (5 mM; Cayman Chemical, 23132), NMN (10 µM; Cayman Chemical, 16411), malic acid (0.5 mM; Sigma-Aldrich, PHR1273), the cell membrane-permeable dimethyl-2-KG (10 mM), GSK-J4 (1 µM; Sigma-Aldrich, SML0701), the cell membrane-permeable octyl-(R)-2 hydroxyglutarate 2-hydroxyglutaric acid (2-HG) (10 mM; Sigma-Aldrich, SML2200) and R162 (20 µM; Sigma-Aldrich, 5380980001) were added as indicated. In some experiments, where indicated, purified T cells were cultured with anti-CD3 and anti-CD28 or NH_4OH (0.977 µM to 8 mM, as indicated in the figures; Santa Cruz, sc-214535).

Staining of human tissue sections and microscopy

Paraffin-embedded slides were deparaffinized and rehydrated before epitope retrieval at 95 °C for 20 min. Slides were then rinsed in cold tap water. Next, slides were stained with anti-GOT1 in a moist chamber at 4 °C overnight. Slides were washed three times in PBS plus 0.1% Triton X-100 before being stained with 2 µg ml^{-1} Alexa Fluor 488-conjugated donkey anti-rabbit secondary antibody for 60 min at room temperature. Slides were washed and stained with Alexa Fluor 647-conjugated anti-CD8a for 60 min at room temperature. Sections were washed and covered with DAPI-containing anti-fade reagent and mounted with a coverslip. A confocal microscope (Zeiss LSM 710, ZEN Black Software) was used to photograph the sections.

Flow cytometry

For surface antigen staining, Fc receptor blockers anti-CD16/CD32 were used to prevent nonspecific antibody binding. Cells were incubated in FACS buffer (PBS supplemented with 0.5% FCS) with the fluorescently conjugated antibodies for 30 min on ice. DAPI or a Live/DEAD Fixable Dead Cell Stain kit (Thermo Fisher) was used to exclude the dead cells. For intracellular cytokine staining, cells were fixed with the fixation buffer containing 4% paraformaldehyde (PFA; BioLegend) first, then

permeabilized with eBioscience permeabilization buffer. For staining nuclear antigens, cells were fixed and permeabilized with the eBioscience Foxp3/transcription factor staining buffer set on ice for at least 30 min. Samples were washed and run on an LSR II or LSR Fortessa flow cytometer. We used FACS Diva Software (version 9, BD Biosciences) to collect FACS data, and analyzed data in FlowJo software (10.1r1).

Antibodies

Following antibodies were obtained from BioLegend: Alexa Fluor 488-conjugated donkey anti-rabbit secondary antibody (406416, 1:2,000), Alexa Fluor 647-conjugated anti-CD8a (clone C8/144B, 372906, 1:200), BV421 anti-mouse CD8a (clone 53-6.7, 100738, 1:200), PE Donkey anti-rabbit IgG (polyclonal, 406421, 1:1,000), PerCP/Cyanine5.5 anti-mouse CD8a (clone 53-6.7, 100734, 1:200), BV711 anti-mouse CD45.1 (clone A20, 110739, 1:400), PE anti-mouse TIGIT (clone 1G99, 142104, 1:400), PE/Cyanine7 anti-mouse PD-1 (clone 29F.1A12, 135216, 1:400), PE anti-mouse TNF (clone MP6-XT22, 506306, 1:400), PE/Cyanine7 anti-mouse IFN-γ (clone XMG1.2, 505826, 1:400), BV421 donkey anti-rabbit IgG (polyclonal, 406410, 1:1,000), BV421 anti-mouse CD4 (clone GK1.5, 100438, 1:200), APC/Cyanine7 anti-mouse CD4 (clone GK1.5, 100414, 1:200), BV42 anti-CD44 (clone IM7, 103040, 1:400), PE/Cyanine7 anti-CD62L (clone MEL-14, 104418, 1:400), APC anti-CD25 (clone 3C7, 101910, 1:400), PE anti-IL-7Rα (clone A7R34, 135010, 1:400), anti-CD16/32 (clone 93, 101330, 1:100), anti-mouse CD3 (clone 17A2, 100238, 2 ug ml^{-1}), anti-mouse CD28 (clone 37.51, 02116, 2 ug ml^{-1}), anti-human CD3 (clone OKT3, 317326, 2 ug ml^{-1}), anti-human CD2 (clone TS1/8, 309236, 2 ug ml^{-1}) and anti-human CD28 (clone CD28.2, 302934, 2 ug ml^{-1}). Following antibodies were obtained from Cell Signaling Technology: anti-GOT1 (clone E4A4O, 34423S, 1:500 for flow cytometry and tissue section stainings, 1:1,000 for immunoblotting), anti-GRP94 (clone D6X2Q, 20292, 1:500), anti-NFAT1 (clone D43B1, 5861, 1:200), anti-Eomes (polyclonal, 4540, 1:200), anti-Blimp1 (clone C14A4, 9115, 1:200), rabbit IgG (polyclonal, 2729, 1:200), Alexa Fluor 488-conjugated anti-Bim (clone C34C5, 94805, 1:400) and anti-Cleaved Caspase-3 (clone 5A1E, 9664, 1:400). Anti-TOX (polyclonal, ab155768, 1:200) is from Abcam. Anti-Ki-67 PE-Vio770 (clone REA183, 130-120-419, 1:400) is from Miltenyi.

Immunoblotting

Cells were lysed with RIPA lysis buffer. Proteins were resolved with 15% SDS-PAGE (70 V for 30 min and then 60–90 min at 100 V, until the blue indicator ran to the edge of the gel). Proteins were subsequently transferred onto PVDF membranes (400 mA, 90 min). The membranes were blocked with 5% BSA in PBS supplemented with Tween-20 (PBST) for 1 h at room temperature, then incubated overnight at 4 °C with anti-GOT1 and anti-GRP94. The PVDF membrane was washed three times with PBST, and then incubated with HRP-conjugated secondary antibodies at room temperature for 1 h. The membrane was developed with the ECL method, and the data were collected with a Fusion system (FX6 Edge, Vilber). We quantified the band intensities in the NIH ImageJ (Version 1.53t) program.

ATAC sequencing

A total of 100,000 viable cells were washed in PBS; subsequently, nuclei were isolated with the cold lysis buffer. Nuclei were resuspended in ATAC tagmentation master mix buffer and incubated at 500*g* for 30 min at 37 °C. Transposed chromatin was purified for subsequent library preparation. Sequencing was performed at the DKFZ Genomics and Proteomics Core Facility on the High Seq 2000 v4 Paired-End 125 bp platform. The DKFZ High Throughput Sequencing Unit prepared and sequenced the library (Illumina NovaSeq 6000 Paired-End Read 100 bp). Briefly, the ATAC-sequencing data were first subjected to adapter trimming and low-quality read filtering with flexbar (version 2.5)[45] with the following parameters: -u 5 -m 26 -ae RIGHT -at 2 -ao 1. The trimmed reads were mapped to the mouse reference genome (mm10) with Bowtie 2 (version 2.4.2)[46] with parameters -X 2000–mm. Reads that mapped to mitochondrial DNA or those with low mapping quality (<30) were excluded from downstream analysis. Duplicate reads due to PCR amplification of single DNA fragments during library preparation were identified with Picard (version 2.17.3; available at http://broadinstitute.github.io/picard) and thus were removed from the downstream analysis. MACS2 (version 2.2.7.1)[47] was used for calling open chromatin regions. To identify peaks with differential accessibility, we counted the deduplicated reads overlapping with peaks. DESeq2 (version 1.30.1)[48] was then used for statistical comparison, with a similar procedure regarding analyzing the RNA-seq data. Peaks with adjusted *P* values less than 0.05 and fold changes above 1.5 were considered the differentially accessible peaks. The ATAC sequencing data have been deposited in the Genome Expression Omnibus database under accession number GSE220876.

RNA sequencing

The DKFZ High Throughput Sequencing Unit prepared and sequenced the library (Illumina NovaSeq 6000 Paired-End Read 50 bp). We analyzed the sequencing data according to a previously described protocol[49]. Briefly, the RNA-sequencing reads were first subjected to adapter trimming and low-quality read filtering with flexbar (version 2.5)[45] with the following parameters: -u 6 -m 36 -ae RIGHT -at 2 -ao 2. Reads that were mapped to the reference sequences of rRNA, tRNA, snRNA, snoRNA and miscRNA (available from Ensembl and RepeatMasker annotation) with Bowtie 2 (version 2.4.2)[46] with default parameters (in --end-to-end & --sensitive mode) were excluded. The remaining reads were then mapped to the mouse reference genome (mm10) with STAR (version 2.7.7a)[50] with key parameters --outFilterMismatchNmax 8 --outFilterMismatchNoverLmax 0.1 -- alignIntronMin 20 --alignIntronMax 1000000 --outFilterType BySJout --outFilterIntronMotifs RemoveNoncanonicalUnannotated. Reads that mapped to multiple genomic sites were discarded in the following analysis. HTSeq-count (version 2.0.1)[51] was used to count reads mapped to annotated genes, with parameters -f bam -r pos -s no -a 10. Differentially expressed gene analysis was performed with the R package DESeq2 (version 1.30.1)[48]. In brief, size factor estimation was first conducted to normalize the data across samples, and this was followed by dispersion estimation to account for the negative binomial distributed count data in RNA sequencing. Finally, gene expression fold changes were calculated, and the significance of the gene expression difference was estimated with the Wald test. To control for the false discovery rate in multiple testing, the raw *P* values were adjusted with the Benjamini–Hochberg procedure. Genes with adjusted *P* values less than 0.05 and fold changes above 1.5 were considered differentially expressed. The RNA-sequencing data have been deposited in the Genome Expression Omnibus database under accession number GSE220876.

ChIP–PCR

We crosslinked DNA and proteins (1% formaldehyde, 12 min), lyzed cells, collected nuclei and resuspended the pellets in 300 µl SDS lysis buffer (1% SDS, 10 mM EDTA, 50 mM Tris–HCl and protease inhibitors). Cells were sonicated (Covaris M220 sonicator, duty factor 15%, peak incident 75 W, 200 cycles per burst, 10 min) to shear chromatin before centrifugation. The supernatants were incubated with antibodies or IgG isotype control and incubated at 4 °C overnight. After that, 50 µl BSA-blocked Dynabeads Protein A/G were incubated with the supernatant at 4 °C overnight. The magnetic beads were washed before the DNA–protein complexes were eluted at (65 °C for 30 min). We then treated the eluted complexes using RNase (10 µg ml^{-1}) and proteinase K (200 µg ml^{-1}) to remove RNA and protein before recovering DNA using the Qiagen PCR purification kit. In the subsequent qPCR analysis (ABI Prism 7500 sequence detection system, Applied Biosystems), we used 3 µl eluted DNA, 5 µl SyberGreen master mixture and 2 µl primers (Source data for Extended Table 1) for each reaction. The abundance of

DNA was calculated using the ΔCt values between immunoprecipitated or input samples.

Quantification of NAD$^+$ and NADH

NAD$^+$ and NADH were determined with an NAD/NADH-Glo Assay kit (Promega, G9071) according to the manufacturer's instructions. Briefly, 10^6 cells were lysed with 30 µl lysis buffer and then split into two fractions. For measurement of NAD$^+$, 15 µl lysate was mixed with 7.5 µl of 0.4 M HCl, incubated at 60 °C for 15 min, and neutralized with 7.5 µl Tris-base. To measure NADH, samples were incubated for 15 min at 60 °C before 15 µl Tris–HCl was added. Subsequently, equal amounts of a luciferin detection reagent were added before the luciferase signal was measured with a luminescence detector. NAD$^+$ and NADH concentrations were calculated with standard curves.

Quantification of the malate shuttle-associated metabolites

To measure the malate shuttle-associated metabolites, we adapted a previously published method[52]. In brief, 10^6 cells were extracted in 100 µl ice-cold methanol with sonication on ice. For derivatization, 50 µl extract was mixed with 25 µl 140 mM 3-nitrophenylhydrazine hydrochloride, 25 µl methanol and 100 µl 50 mM ethyl-3-(3-dimethylaminopropyl) carbodiimide hydrochloride, and incubated for 20 min at 60 °C. Samples were separated by reversed-phase chromatography on an Acquity H-class UPLC system coupled to a QDa mass detector (Waters) with an Acquity HSS T3 column (100 mm × 2.1 mm, 1.8 µm, Waters), which was heated to 40 °C. Separation of derivatives was achieved by increasing the concentration of 0.1% formic acid in acetonitrile (B) in 0.1% formic acid in water (A) at 550 µl min^{-1} as follows: 2 min 15% B, 2.01 min 31% B, 5 min 54% B, 5.01 min 90% B, hold for 2 min and return to 15% B in 2 min. Mass signals for the following compounds were detected in single ion record mode by using negative detector polarity and 0.8 kV capillary voltage: malate (403.3 *m/z*; 25 V CV), succinate (387.3 *m/z*; 25 CV), fumarate (385.3 *m/z*; 30 V), citrate (443.3 *m/z*; 10 V), pyruvate (357.3 *m/z*; 15 V) and α-ketoglutarate (550.2 *m/z*; 25 CV). Data acquisition and processing were performed with the Empower3 software suite (Waters).

Quantification of ammonia in CD8$^+$ T cells

We used an Ammonia Assay Kit (Sigma-Aldrich, AA0100). We centrifuged cells (750*g*, 5 min, 4 °C), and lysed cells in 0.5% Triton X-100 on ice for 10 min. Subsequently, 20 µl lysate was mixed with 200 µl ammonia assay reagent and incubated at room temperature for 5 min. We then measured the absorbance at 340 nm with a spectrophotometer. We subsequently added 2 µl of L-GDH solution (in the Ammonia Assay Kit) to each well, gently mixed each well and incubated for 5 min at room temperature. The absorbance of each solution at 340 nm was again determined with a spectrophotometer. We obtained the ΔA340 value, and further calculated the amount of ammonia according to the instructions of the kit. Cell mass was quantified with graduated packed cell volume tubes (TPP Techno Plastic Products AG; Trasadingen, 870005). We divided the total amount of ammonia by the CD8$^+$ T cell mass to calculate the concentrations of ammonia in cells.

Metabolic tracer labeling

T cells were FACS-purified, pelleted and resuspended in PBS containing 1% FBS (1×10^6 cells per ml, 0.5 ml). Tracers, including 2 mM $^{13}C_5$-glutamine (Sigma-Aldrich, 605166), 1 mM $^{15}NH_4Cl$ (Sigma-Aldrich, 299251) and 0.5 mM $^{13}C_4$-malic acid (Sigma-Aldrich, 750484), were added individually to the cells. Subsequently, 20 µM GDH1 inhibitor R162 (Calbiochem, 538098) was added as indicated. After 2 h, the labeling was quenched with cold 0.9% NaCl, and the tracers were washed out. The cell pellets were submitted to the Heidelberg Center for Organismal Studies and subjected for general tracing analysis to gas chromatography/mass spectrometry (GC/MS) and for glutamine, glutamate and alanine tracing analysis to liquid chromatography coupled to Ion Mobility Separation with Quadrupole Time of Flight (LC-IMS QTOF). For GC/MS analysis, frozen pellets of 10^6 cells were extracted with 190 µl of 100% methanol (15 min, 70 °C). Each sample was mixed with 100 µl chloroform and shaken at 37 °C for 5 min. Then 200 µl water was added, and the samples were centrifuged (10 min, 11,000*g*) to separate polar and organic phases. The upper polar phase (300 µl) was transferred to a fresh tube before being dried in a vacuum concentrator. Sequential online methoximation and silylation reactions were performed using a MPS autosampler (Gerstel). Methoximation was performed by adding 20 µL 20 mg ml^{-1} methoxyamine hydrochloride (Sigma-Aldrich, 226904) in pyridine (Sigma-Aldrich, 270970) and incubation at 37 °C for 90 min in a Gerstel MPS Agitator Unit. For silylation reactions, 45 µl of N-methyl-N-(trimethylsilyl)trifluoroacetamide (MSTFA; Sigma-Aldrich, 69479) was added and samples were incubated at 37 °C for 30 min with gentle shaking. Before injection, samples were incubated at RT for 45 min. For GC/MS analysis, a GC-ToF system was used consisting of an Agilent 7890 Gas Chromatograph (Agilent) fitted with a Rxi-5Sil MS column (30 m × 0.25 mm × 0.25 µm; Restek Corporation) coupled to a Pegasus BT Mass Spectrometer (LECO Corporation). The GC was operated with an injection temperature of 250 °C and 1 µl sample was injected in splitless mode. The GC temperature program started with a 1 min hold at 40 °C followed by a 6 °C min^{-1} ramp up to 210 °C, a 20 °C min^{-1} ramp up to 330 °C and a bake-out at 330 °C for 5 min using Helium as carrier gas with constant linear velocity. The ToF MS was operated with ion source and interface temperature of 250 °C, a solvent cut time of 12 min and a scan range (*m/z*) of 50–600 with an acquisition rate of 17 spectra per second. Mass isotopologue distribution (MID) was determined using the DExSI software (version 1.11)[53].

Determination of ^{15}N tracer incorporation was done similarly as described[54]. Alanine, glutamate and glutamine content was analyzed after specific labeling with the fluorescence dye AccQ-Tag (Waters) according to the manufacturer's protocol using an Acquity I-class UPLC system coupled to a VION Ion Mobility Separation QTof (Waters). Separation was carried out using a Cortecs C18 column (100 mm × 2.1 mm, 1.6 µm, Waters) at 40 °C. The mobile UPLC phase consisted of binary gradients of ACN with 0.1% formic acid (B) and 0.1% aqueous formic acid (A), flowing at 0.5 ml min^{-1}. Analytes were initially eluted with 98% A and A was decreased linearly to 76% over 7.90 min. After this, the column was washed with 90% B for 1.49 min and re-equilibrated under the initial conditions for 2.9 min. Measurements were performed with an ESI source operated in positive mode (1.00 kV capillary voltage; source temperature 120 °C, desolvation temperature 550 °C; sample cone voltage 20 V; source offset voltage 50 V; observed *m/z* 150–700 Da with a scan time of 0.300 s). Unifi software (Waters) was used to control the instrument and to acquire and process the MS data.

Seahorse extracellular flux analysis

The Seahorse sensor cartridges were hydrated overnight at 37 °C before the assay, according to the manufacturer's instructions. The culture plates were coated with poly D-lysine at 4 °C. To perform electron flow assay, we seeded T cells in mitochondrial assay solution (0.15×10^6 cells per well) supplemented with 4 mM ADP, 2 µM FCCP, 10 mM sodium pyruvate, 2 mM malic acid and 1 nM PMP. The following compounds were injected into the culture plate sequentially: rotenone (2 µM), sodium succinate (10 mM), antimycin A (4 µM) and a mixture of 10 mM Asc and 100 µM TMPD. OCR values were recorded automatically with a Seahorse flux analyzer.

Statistical analysis

No statistical methods were used to predetermine sample sizes but our sample sizes are similar to those reported in previous publications[2,55]. We used GraphPad Prism (v7.0.3) to perform statistical analysis. When comparing two groups, we first determined whether the data points were normally distributed. Statistical analysis of normally distributed data was performed with two-tailed Student's *t* tests. Statistical analysis

of data points that were not normally distributed was performed with two-tailed Mann–Whitney *U* tests (also known as the Wilcoxon rank sum test). Simultaneous comparisons of more than two groups were performed with one-way or two-way analysis of variance, as indicated in the figure legends. In all cases, $P < 0.05$ was considered statistically significant. Sample sizes are indicated in the figure legends. Data are presented as mean ± s.d., as specified in the figure legends. Data collection and analysis were not performed blind to the conditions of the experiments. We did not use a randomization protocol and assigned mice to experimental groups according to genotypes.

Reporting summary

Further information on research design is available in the Nature Portfolio Reporting Summary linked to this article.

Data availability

RNA- and ATAC-sequencing data have been deposited in the GEO database under the accession code GSE220876. All other data are present in the manuscript and the Supplementary Information or from the corresponding authors upon reasonable request. Source data are provided with this paper.

References

43. Pircher, H., Bürki, K., Lang, R., Hengartner, H. & Zinkernagel, R. M. Tolerance induction in double specific T-cell receptor transgenic mice varies with antigen. *Nature* **342**, 559–561 (1989).
44. Seki, A. & Rutz, S. Optimized RNP transfection for highly efficient CRISPR/Cas9-mediated gene knockout in primary T cells. *J. Exp. Med.* **215**, 985–997 (2018).
45. Dodt, M., Roehr, J. T., Ahmed, R. & Dieterich, C. FLEXBAR-flexible barcode and adapter processing for next-generation sequencing platforms. *Biology (Basel)* **1**, 895–905 (2012).
46. Langmead, B. & Salzberg, S. L. Fast gapped-read alignment with Bowtie 2. *Nat. Methods* **9**, 357–359 (2012).
47. Zhang, Y. et al. Model-based analysis of ChIP–seq (MACS). *Genome Biol.* **9**, R137 (2008).
48. Love, M. I., Huber, W. & Anders, S. Moderated estimation of fold change and dispersion for RNA-seq data with DESeq2. *Genome Biol.* **15**, 550 (2014).
49. Wu, J. et al. Loss of neurological disease HSAN-I-associated gene SPTLC2 impairs $CD8^+$ T cell responses to infection by inhibiting T cell metabolic fitness. *Immunity* **50**, 1218–1231 (2019).
50. Dobin, A. et al. STAR: ultrafast universal RNA-seq aligner. *Bioinformatics* **29**, 15–21 (2013).
51. Anders, S., Pyl, P. T. & Huber, W. HTSeq-a Python framework to work with high-throughput sequencing data. *Bioinformatics* **31**, 166–169 (2015).
52. Uran, S., Landmark, K. E., Hjellum, G. & Skotland, T. Quantification of 13C pyruvate and 13C lactate in dog blood by reversed-phase liquid chromatography-electrospray ionization mass spectrometry after derivatization with 3-nitrophenylhydrazine. *J. Pharm. Biomed. Anal.* **44**, 947–954 (2007).
53. Dagley, M. J. & McConville, M. J. DExSI: a new tool for the rapid quantitation of 13C-labelled metabolites detected by GC–MS. *Bioinformatics* **34**, 1957–1958 (2018).
54. Weger, B. D. et al. Extensive regulation of diurnal transcription and metabolism by glucocorticoids. *PLoS Genet.* **12**, e1006512 (2016).
55. Wu, J. et al. Skeletal muscle antagonizes antiviral $CD8^+$ T cell exhaustion. *Sci. Adv.* **6**, eaba3458 (2020).

Acknowledgements

Tissue samples were provided by the tissue bank of the German Center for Infection Research (DZIF, Heidelberg, Germany) in accor dance with the regulations of the tissue bank and the approval of the ethics committee of Heidelberg University. A.M. is supported by the Helmholtz International Graduate School. HPLC-based metabolite quantification was supported partly by the Metabolomics Core Technology Platform of the Excellence Cluster 'CellNetworks' (University of Heidelberg) and the Deutsche Forschungsgemeinschaft (grant ZUK 40/2010-3009262). J.W. is supported by funding from the Institute of Health and Medicine, Hefei Comprehensive National Science Center. X.W. is supported by the National Natural Science Foundation of China (32170742), the Start Fund for Specially Appointed Professor of Jiangsu Province and the Start Fund for High-level Talents of Nanjing Medical University (NMUR2020009). G.C. is supported by a CRI Lloyd J. Old STAR Award (3914), a Helmholtz Young Investigator Award (VH-NG-1113), an EMBO Young Investigator Award, an Exploration grant of the Boehringer Ingelheim Foundation (BIS), the German Research Foundation (DFG; CU375/5-1, CU375/5-2, CU375/7-1, CU375/9-1 and 259332240/RTG2099), the German Cancer Aid Foundation (DKH; 70113343 and 70114224), the Helmholtz Zukunftsthema Ageing and Metabolic Programming (AMPro; ZT0026), HI-TRON Kick-Start Seed Funding (HITR-2021–08), the Hector Foundation (M20102) and an ERC Consolidator Award (101045416).

Author contributions

N.W., J.W., X.W. and G.C. designed the experiments. N.W., S.M., Y.M., A. Madi, A. Mieg, M.H., F.Z., K.M., N.B., D.S., M.B., G.P., G.K., M.S., N.K., C.K. and I.K. performed the biological experiments. X.W. performed the bioinformatics analysis. N.W. and G.C. analyzed the biological data. G.C. wrote the manuscript with input from the other authors.

FundingInformation

Open access funding provided by Deutsches Krebsforschungszentrum (DKFZ).

Competing interests

G.C. declares funding from Bayer, but this funding is not relevant to the present study. The other authors declare no competing interests.

Additional information

Extended data is available for this paper at https://doi.org/10.1038/s41590-023-01636-5.

Supplementary information The online version contains supplementary material available at https://doi.org/10.1038/s41590-023-01636-5.

Correspondence and requests for materials should be addressed to Jingxia Wu, Xi Wang or Guoliang Cui.

Peer review information *Nature Immunology* thanks Ping-Chih Ho and Greg Delgoffe for their contribution to the peer review of this work. Primary Handling Editor: N. Bernard, in collaboration with the *Nature Immunology* team.

https://doi.org/10.1038/s41590-023-01636-5

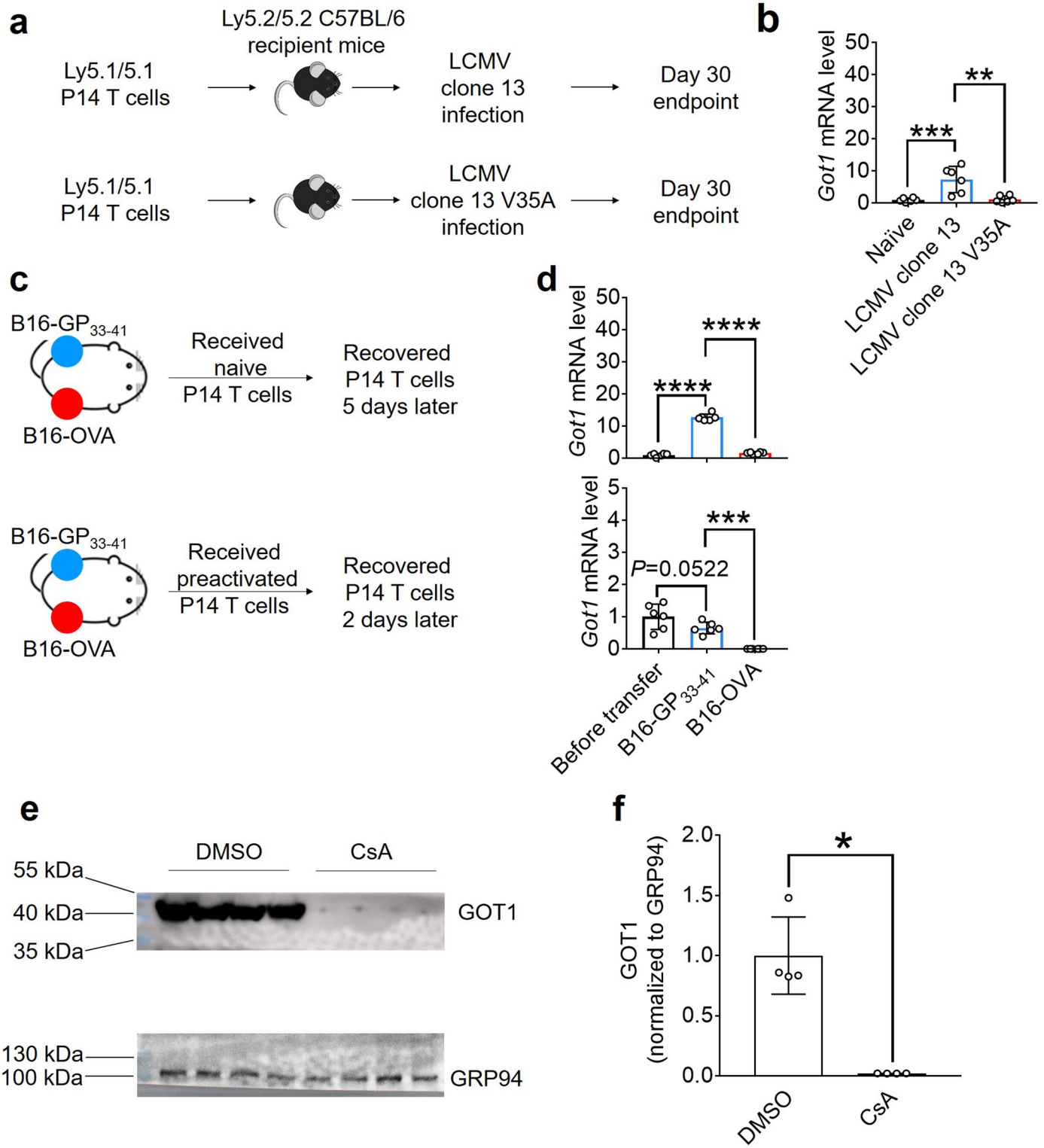

Extended Data Fig. 1 | Antigenic stimulation induces GOT1 expression in CD8$^+$ T cells. a, Illustration of the experimental design of **b**. **b**, A bar graph shows *Got1* mRNA expression in P14 T cells recovered from host mice infected with LCMV clone 13 or LCMV clone 13 V35A (the valine residue at position 35 was replaced with alanine), as quantified by qRT-PCR analysis. **c**, Illustration of the experimental design of **d**. **d**, A bar graph shows *Got1* mRNA expression in P14 T cells before transfer and in P14 T cells recovered from tumors, as quantified by qRT-PCR analysis. **e**,**f**, P14 splenocytes were cultured with the GP_{33-41} peptide for 3 days with or without cyclosporin A (CsA, 5 μM) before western blot analysis (**e**). The bar graph shows the results of densitometric quantification of the immunoblot bands (**f**). GRP94 was used as a loading control. The results are presented as mean ± s.d. *P<0.05; **P<0.01; ***P<0.001; ****P<0.0001. Comparisons were performed with one-way ANOVA (**b** and **d**) or the two-tailed Mann-Whitney test (**f**, data points were not normally distributed). N = 6 mice (**b** and **d**) or N = 4 (**e**–**f**) in each group. P values in **b** (from left to right): 0.0009, 0.001; in **d** (top): both P values <1.0×10^{-15}; in **d** (bottom): 0.0522, 0.0009; in **f**: 0.0286. Seven-week-old female mice were used (**b**, **d**, **e**, **f**).

https://doi.org/10.1038/s41590-023-01636-5

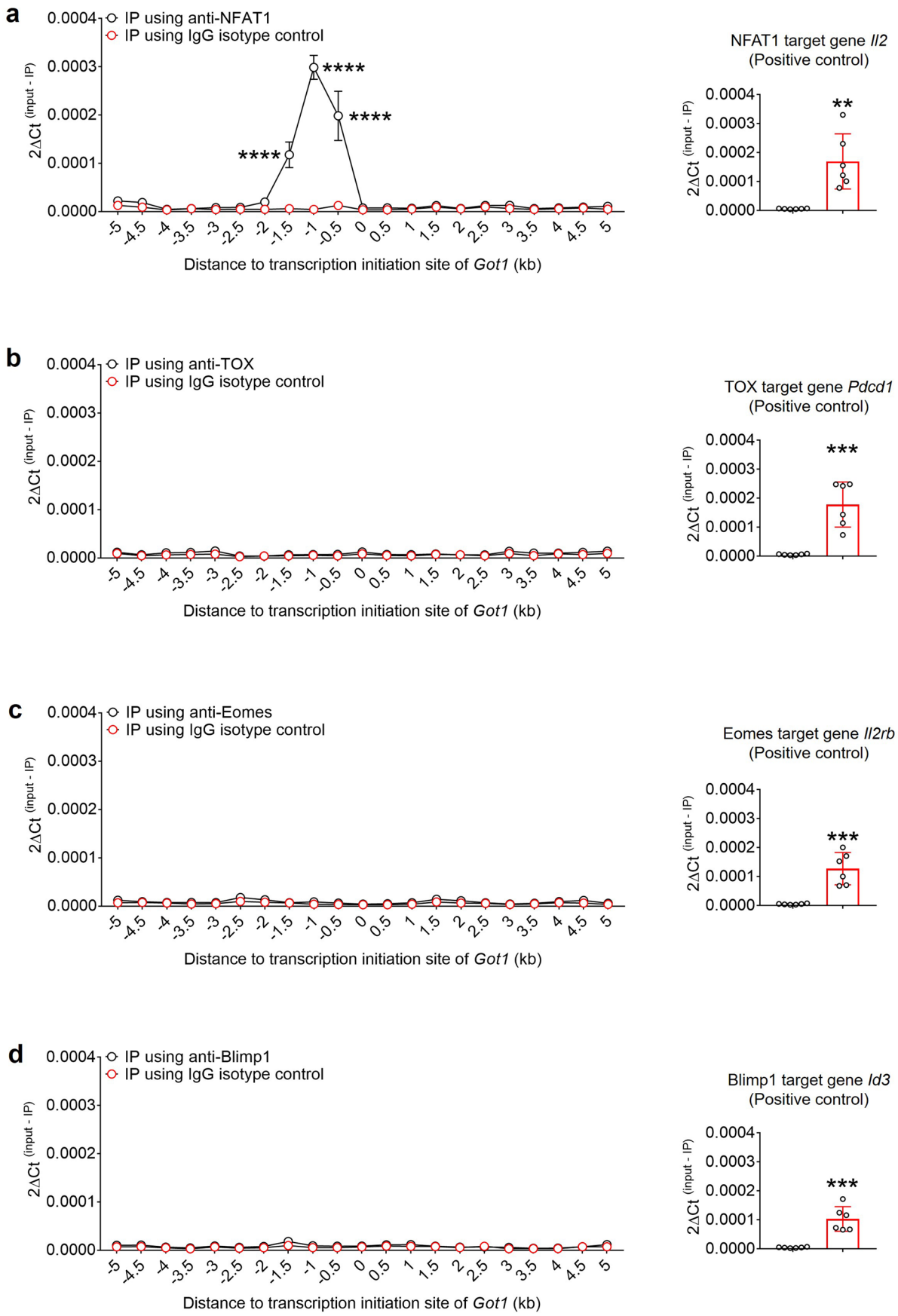

Extended Data Fig. 2 | See next page for caption.

https://doi.org/10.1038/s41590-023-01636-5

Extended Data Fig. 2 | NFAT1 binds to *Got1* locus. a–**d**, P14 splenocytes were cultured with $GP_{33–41}$ peptide for 3 days before ChIP-PCR analysis. PCR was performed using primers evenly spaced across a 10kb region of *Got1* locus. Line curves show the relative quantification results of DNA fragments pulled down using indicated antibodies or IgG isotype control. Bar graphs show the binding of NFAT1 to *Il2* (a known target gene of NFAT1) locus, the binding of TOX to *Pdcd1* (a known target gene of TOX) locus, the binding of Eomes to *Il2rb* (a known target gene of Eomes) locus, and the binding of Blimp1 to *Id3* (a known target gene of blimp1) locus. The data are presented as mean ± s.d. ***P*<0.01; ****P*<0.001; *****P*<0.0001. Comparisons were performed with two-way ANOVA (line graphs, **a**–**d**), a two-tailed Student's *t*-test (bar graphs, **a**–**d**, data points were normally distributed). *P* values in **a** (from left to right): 9.1×10^{-13}, $<1.0 \times 10^{-15}$, $<1.0 \times 10^{-15}$, 0.002; **b**: 0.0003; **c**: 0.0003; in **d**: 0.0002. Seven-week-old male mice were used (**a**–**d**).

https://doi.org/10.1038/s41590-023-01636-5

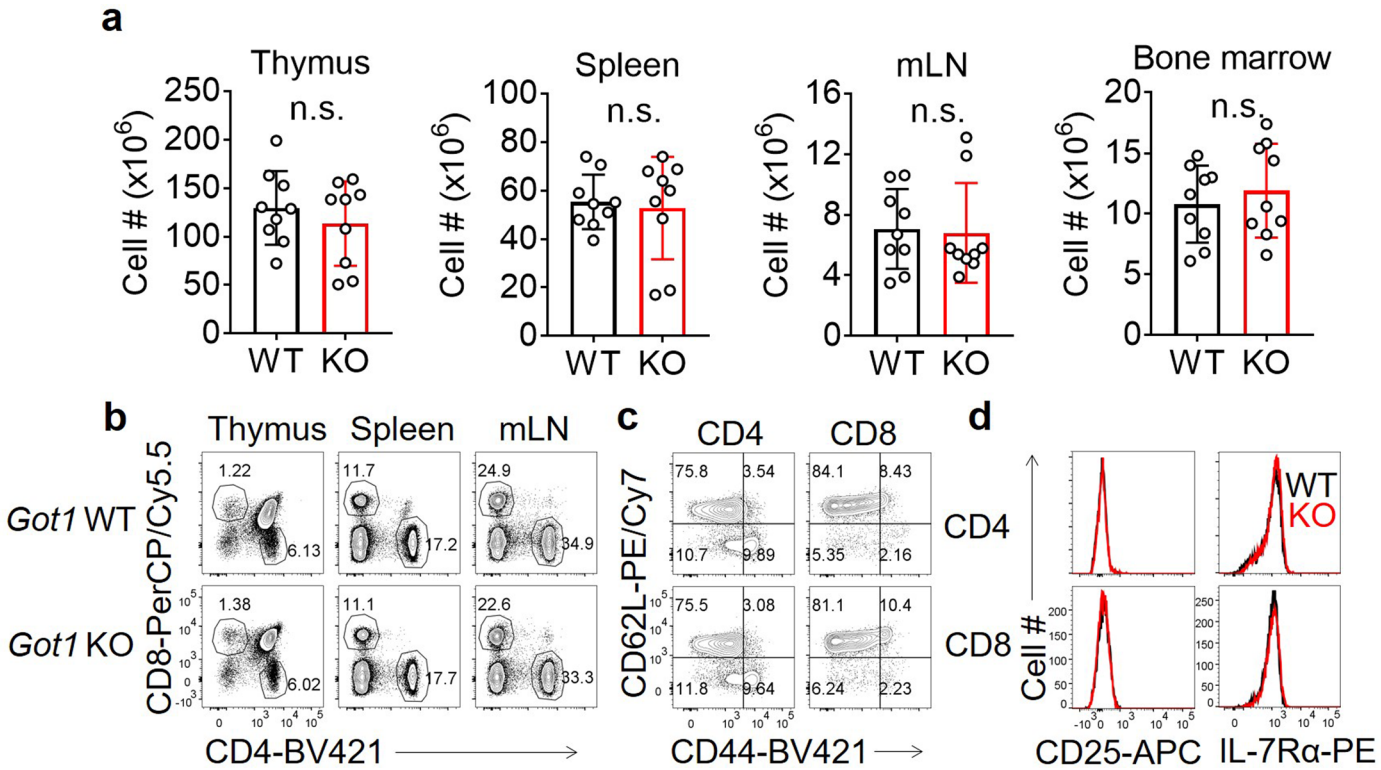

Extended Data Fig. 3 | Basic immune characterization of *Got1*-deficient mice. a, Bar graphs show the numbers of thymocytes, splenocytes, mesenteric lymphocytes (mLNs), and bone marrow cells in littermates. **b**, Flow cytometry dot plots show the percentages of $CD4^+$ and $CD8^+$ T cells in thymocytes, mLNs, and splenocytes. **c**, The percentages of splenic $CD4^+$ and $CD8^+$ T cells expressing CD44 and CD62L are shown. **d**, Flow cytometry histograms show the expression of CD25 and IL-7Rα in splenic $CD4^+$ and $CD8^+$ T cells. The data are expressed as mean ± s.d. and are cumulative (**a**) or representative (**b**–**d**) data from two independent experiments with nine pairs of littermates. n.s., not significant. Comparisons were performed with a two-tailed Student's *t*-test (**a**, data points were normally distributed). *P* values in **a** (from left to right): 0.414, 0.751, 0.852, 0.516. Six to seven-week-old female mice were used (**a**–**d**).

https://doi.org/10.1038/s41590-023-01636-5

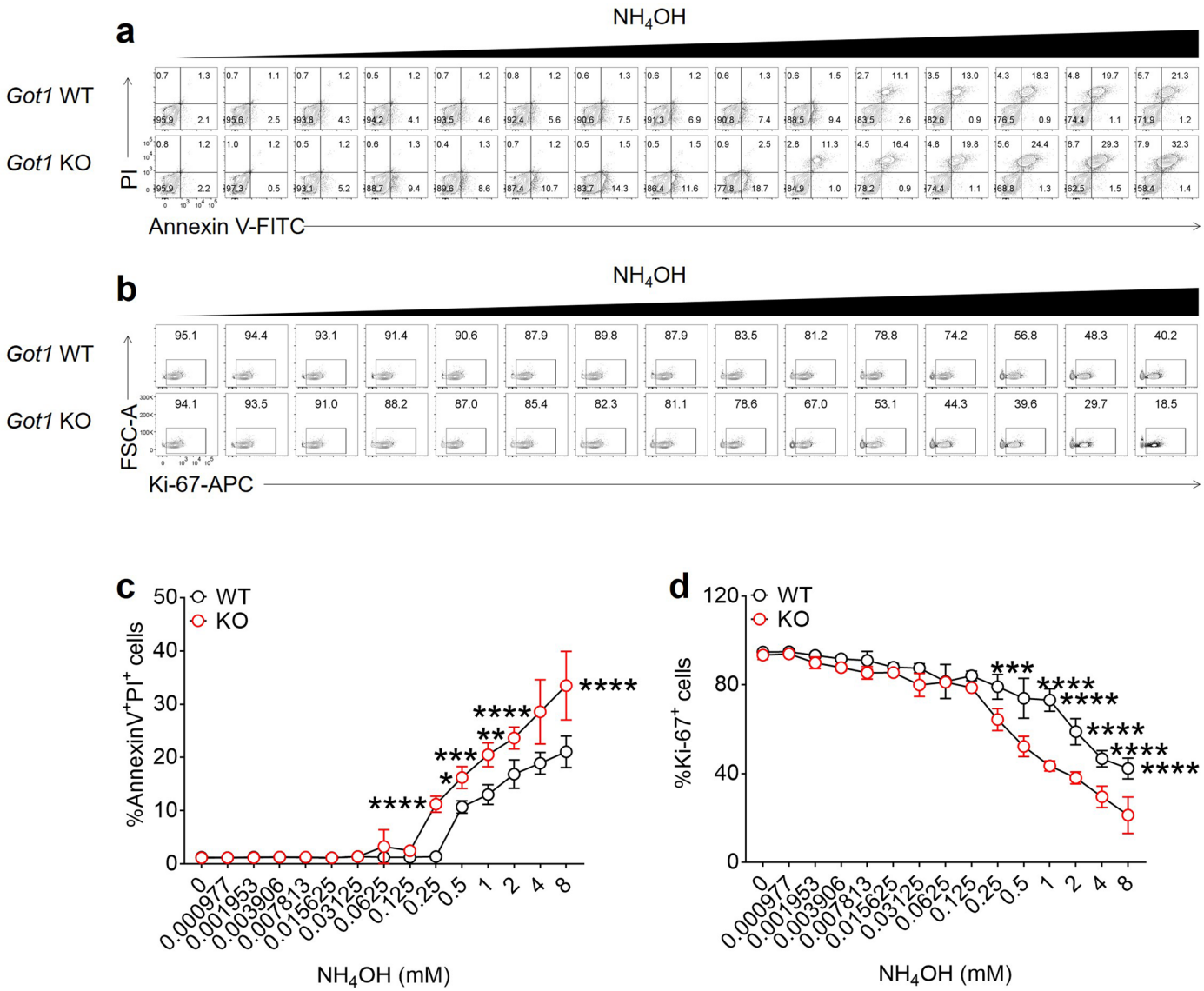

Extended Data Fig. 4 | Ammonia promotes T cell apoptosis and inhibits T cell proliferation. a–**d**, *Got1*-deficient and -sufficient donor P14 $CD8^+$ T cells were isolated from C57BL/6 host mice infected with LCMV Armstrong 8 days earlier. A total of 0.25×10^6 cells were cultured with anti-CD3 and anti-CD28 in the presence or absence of NH_4OH for 2 days. FACS plots (**a**–**b**) and line graphs (**c**–**d**) show the percentages of $AnnexinV^+$ PI^+ cells (**a**, **c**) and Ki-67^+ cells (**b**, **d**). Data are combined from two experiments with three mice in total. The results are presented as mean ± s.d. **P*<0.05; ***P*<0.01; ****P*<0.001; *****P*<0.0001. Comparisons were performed using two-way ANOVA. *P* values in **c** (from left to right): 3.6×10^{-6}, 0.026, 0.0006, 0.003, 5.3×10^{-6}, 9.7×10^{-9}; in **d**: 0.0006, 2.3×10^{-7}, 1.9×10^{-11}, 6.3×10^{-7}, 4.0×10^{-5}, 4.8×10^{-7}. Six-week-old female mice were used (**a**–**d**).

https://doi.org/10.1038/s41590-023-01636-5

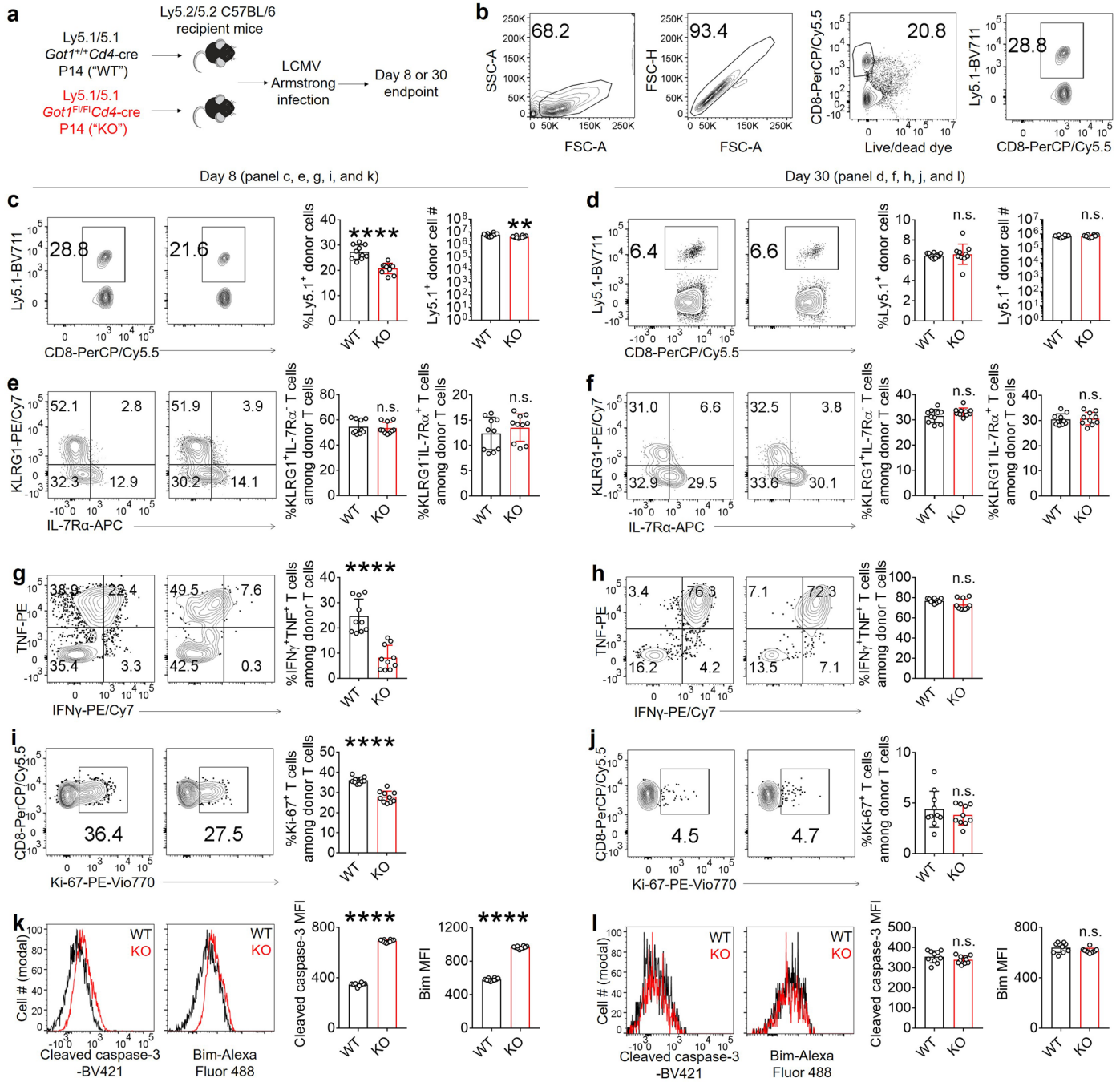

Extended Data Fig. 5 | CD8⁺ T cell responses require GOT1 during acute infection. a, Experimental design illustration. **b**, FACS gating strategies used in **c**–**l**. **c**–**l**, Contour plots, histograms, and bar graphs show the flow cytometry staining results of Ly5.1⁺ donor P14 CD8⁺ T cells (**c**,**d**), KLRG1 and IL-7Rα (**e**,**f**), cytokines (**g**,**h**), Ki-67 (**i**,**j**), and cleaved caspase-3 and Bim (**k**–**l**) in *Got1*-deficient and sufficient P14 CD8⁺ T cells. Cells were stimulated with GP_{33-41} peptide before the flow cytometry staining (**g**,**h**). Data were pooled from two independent experiments (**c**–**l**) with ten C57BL/6 mice in each group receiving *Got1*-deficient and sufficient donor P14 CD8⁺ T cells. The results are presented as mean ± s.d. $^{**}P<0.01$; $^{***}P<0.001$; $^{****}P<0.0001$; n.s., not significant. Comparisons were performed using a two-tailed Student's *t*-test (**c**, **d**, %KLRG1⁻IL-7Ra⁺ T cells among donor T cells in **e**, **f**, **g**, **h**, **i**, **j**, **k**, **l**; data points were normally distributed) or the two-tailed Mann-Whitney test (%KLRG1⁺IL-7Ra⁻ T cells among donor T cells in **e**; data points were not normally distributed). *P* values in **c**: 1.6×10^{-5}, 0.006; in **d**: 0.675, 0.745; in **e**: 0.752, 0.397; in **f**: 0.127, 0.738; in **g**: 6.4×10^{-6}; in **h**: 0.069; in **i**: 2.4×10^{-4}; in **j**: 0.3959; in **k**: 1.1×10^{-5}, $<1.0\times10^{-15}$; in **l**: 0.194, 0.088. Six-week-old female mice were used (**b**–**l**).

https://doi.org/10.1038/s41590-023-01636-5

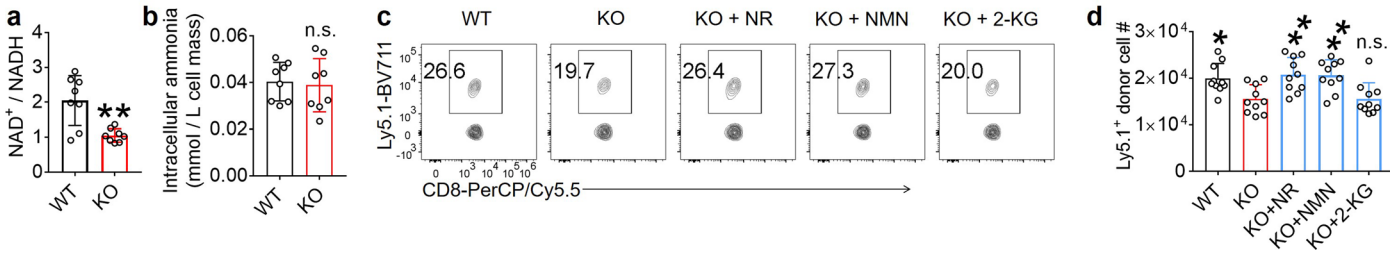

Extended Data Fig. 6 | GOT1 maintains the NAD$^+$/NADH ratio in acute LCMV infections. a,**b**, Bar graphs display NAD$^+$/NADH ratios (**a**) and amounts of ammonia (**b**) in *Got1*-deficient and sufficient donor P14 CD8$^+$ T cells isolated from C57BL/6 host mice infected 8 days earlier with LCMV Armstrong. **c**,**d**, Splenocytes were isolated from host mice 8 days after LCMV Armstrong infection and cultured with GP_{33-41} peptide in the presence or absence of the indicated compounds for 1 day. Flow cytometry contour plots (**c**) and a bar graph (**d**) show the percentages of *Got1*-deficient and sufficient Ly5.1$^+$ donor T cells among CD8$^+$ host T cells. Data are combined from two experiments with eight (**a**–**b**) or ten (**d**) mice in total. The data are presented as mean ± s.d. *P<0.05; **P<0.01; n.s., not significant. Comparisons were performed using a two-tailed Student's t-test (**a** and **b**; data points were normally distributed) and one-way ANOVA (**d**). P values in **a**: 0.002; in **b**: 0.760; in **d**: 0.017, 0.004, 0.005, >0.9999. Six-week-old female mice were used (**a**–**d**).

https://doi.org/10.1038/s41590-023-01636-5

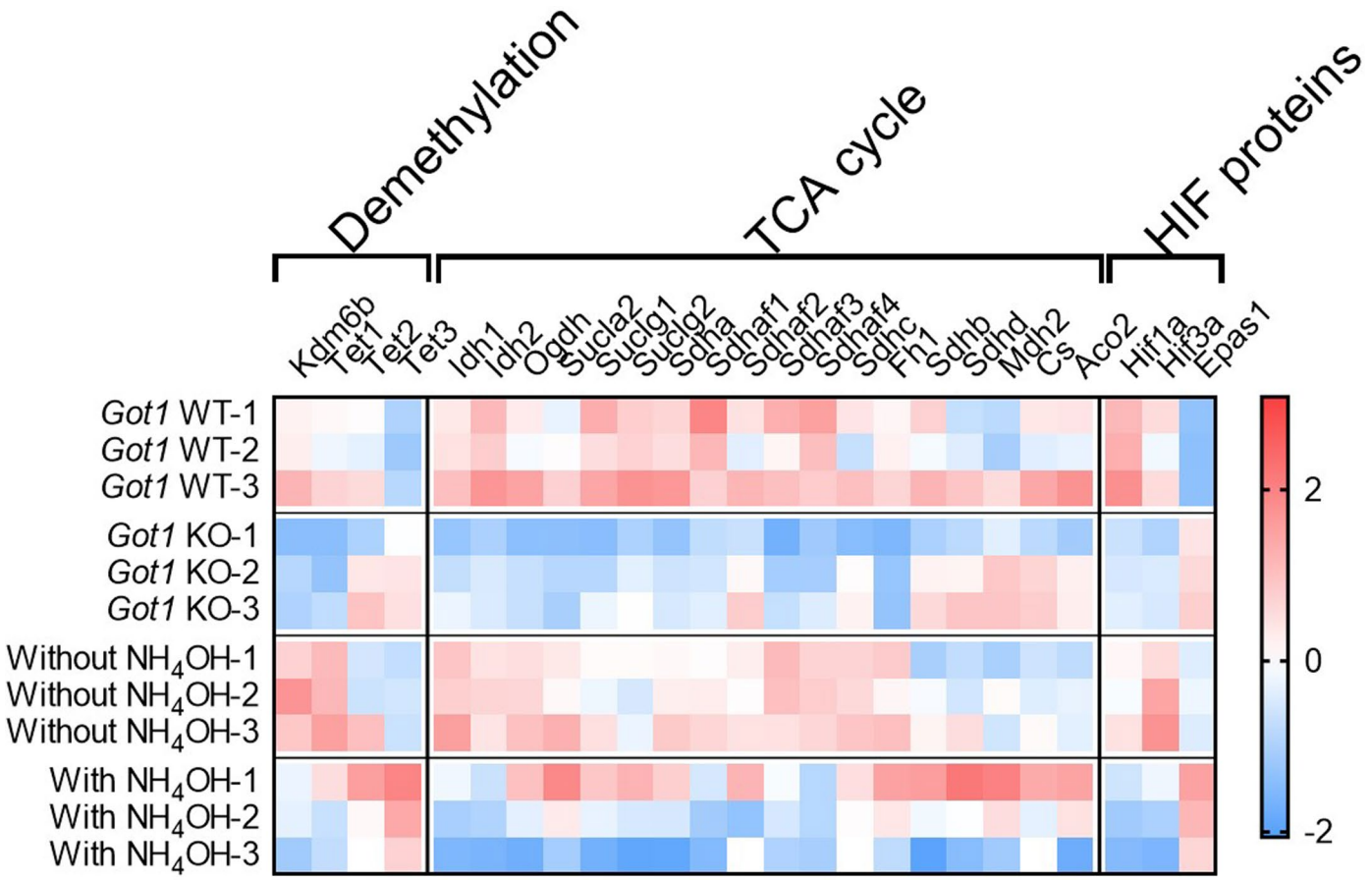

Extended Data Fig. 7 | *Got1* and ammonia influence the expression of 2-KG-related genes. *Got1*-deficient and sufficient donor P14 $CD8^+$ T cells were isolated from C57BL/6 host mice infected with LCMV clone 13 8 days earlier, similar to those described in Fig. 4. *Got1*-deficient P14 cells and *Got1*-sufficient P14 cells were used for RNA sequencing and ATAC sequencing analyses. The heat map shows the mRNA expression z-scores of the indicated genes in the four groups of cells. N = 3 mice in each of the four groups. Six-week-old male mice were used.

nature portfolio

Corresponding author(s): Guoliang Cui

Last updated by author(s): Aug 24, 2023

Reporting Summary

Nature Portfolio wishes to improve the reproducibility of the work that we publish. This form provides structure for consistency and transparency in reporting. For further information on Nature Portfolio policies, see our Editorial Policies and the Editorial Policy Checklist.

Statistics

For all statistical analyses, confirm that the following items are present in the figure legend, table legend, main text, or Methods section.

n/a	Confirmed
☐	☒ The exact sample size (*n*) for each experimental group/condition, given as a discrete number and unit of measurement
☐	☒ A statement on whether measurements were taken from distinct samples or whether the same sample was measured repeatedly
☐	☒ The statistical test(s) used AND whether they are one- or two-sided *Only common tests should be described solely by name; describe more complex techniques in the Methods section.*
☒	☐ A description of all covariates tested
☐	☒ A description of any assumptions or corrections, such as tests of normality and adjustment for multiple comparisons
☐	☒ A full description of the statistical parameters including central tendency (e.g. means) or other basic estimates (e.g. regression coefficient) AND variation (e.g. standard deviation) or associated estimates of uncertainty (e.g. confidence intervals)
☐	☒ For null hypothesis testing, the test statistic (e.g. *F*, *t*, *r*) with confidence intervals, effect sizes, degrees of freedom and *P* value noted *Give P values as exact values whenever suitable.*
☒	☐ For Bayesian analysis, information on the choice of priors and Markov chain Monte Carlo settings
☒	☐ For hierarchical and complex designs, identification of the appropriate level for tests and full reporting of outcomes
☒	☐ Estimates of effect sizes (e.g. Cohen's *d*, Pearson's *r*), indicating how they were calculated

Our web collection on statistics for biologists contains articles on many of the points above.

Software and code

Policy information about availability of computer code

Data collection

We used FACS Diva Software (version 9, BD Biosciences) to collect FACS data.
FACS data were analyzed using FlowJo software (10.1r1).
Western blot data were collected by Fusion (FX6 Edge, Vilber).
We used the ABI Prism 7500 sequence detection system (SDS Software v1.2.3, Applied Biosystems) to collect the qPCR data.
We quantified the band intensities in the NIH ImageJ program (Version 1.53t).
Mass isotopologue distribution (MID) was determined using the DExSI software (Version 1.11).

Data analysis

FACS data were analyzed using Flowjo software (version 10.1rl). Western blot data were analyzed using Fusion FX6 Edge.
RNA sequencing reads were first subjected to adapter trimming and low-quality read filtering with flexbar (version 2.5) with the following parameters: -u 6 -m 36 -ae RIGHT -at 2 -ao 2. Reads that were mapped to the reference sequences of rRNA, tRNA, snRNA, snoRNA, and miscRNA (available from Ensembl and RepeatMasker annotation) with Bowtie 2 (version 2.4.2) with default parameters (in --end-to-end &--sensitive mode) were excluded. The remaining reads were then mapped to the mouse reference genome (mml0) with STAR (version 2.7.7a) with key parameters --outFilterMismatchNmax 8--outFilterMismatchNoverlmax 0.1-- alignIntronMin 20--alignIntronMax 1000000--outFilterType BySJout --outFilterIntronMotifs RemoveNoncanonicalUnannotated. Reads that mapped to multiple genomic sites were discarded in the following analysis. HTSeq-count (version 2.0.1) was used to count reads mapped to annotated genes, with parameters -f barn -r pos -s no -a 10. Differentially expressed gene analysis was performed with the R package DESeq2 (version 1.30.1). In brief, size factor estimation was first conducted to normalize the data across samples, and this was followed by dispersion estimation to account for the negative binomial distributed count data in RNA sequencing. Finally, gene expression fold changes were calculated, and the significance of the gene expression difference was estimated with the Wald test. To control for the false discovery rate in multiple testing, the raw p-values were adjusted with the Benjamini-Hochberg procedure.

ATAC sequencing data were first subjected to adapter trimming and low-quality read filtering with flexbar (version 2.5) with the following parameters: -u 5 -m 26 -ae RIGHT -at 2 -ao 1. The trimmed reads were mapped to the mouse reference genome (mmlO) with Bowtie 2 (version 2.4.2) with parameters -X 2000 --mm. Reads that mapped to mitochondrial DNA or those with low mapping quality(< 30) were excluded from downstream analysis. Duplicate reads due to PCR amplification of single DNA fragments during library preparation were identified with Picard (version 2.17.3; available at http://broadinstitute.github.io/picard) and thus were removed from the downstream analysis. MACS2 (version 2.2.7.1) was used for calling open chromatin regions. To identify peaks with differential accessibility, we counted the deduplicated reads overlapping with peaks. DESeq2 (version 1.30.1),

For manuscripts utilizing custom algorithms or software that are central to the research but not yet described in published literature, software must be made available to editors and reviewers. We strongly encourage code deposition in a community repository (e.g. GitHub). See the Nature Portfolio guidelines for submitting code & software for further information.

Data

Policy information about availability of data

All manuscripts must include a data availability statement. This statement should provide the following information, where applicable:

- Accession codes, unique identifiers, or web links for publicly available datasets
- A description of any restrictions on data availability
- For clinical datasets or third party data, please ensure that the statement adheres to our policy

The GEO accession number for the RNA sequencing data and ATAC sequencing data is GSE220876. The dataset will become public from September 1, 2023. All data needed to evaluate the conclusions in the paper are present in the manuscript and the Supplementary Information. There are no data restrictions.

Research involving human participants, their data, or biological material

Policy information about studies with human participants or human data. See also policy information about sex, gender (identity/presentation), and sexual orientation and race, ethnicity and racism.

Reporting on sex and gender	For the in vitro culture studies: buffy coat human peripheral blood mononuclear cell (PBMC) samples from healthy donors were provided by the blood bank of Mannheim. There were 4 male donors and 4 female donors. We did not observe different phenotypes between the male and female donor T cells. For the HIV patient tissue section studies: lymph node sections were provided by the tissue bank of the German Center for Infection Research. HIV-positive samples were from 2 male donors (59-year-old, 62-year-old) and 1 female donor (34-year-old). HIV-negative samples were also from 2 male donors (65-year-old, 74-year-old) and 1 female donor (51-year-old).
Reporting on race, ethnicity, or other socially relevant groupings	We did not consider the information of race, ethnicity, or other socially relevant groupings when we requested samples from the blood bank of Mannheim or from the tissue bank of the German Center for Infection Research (DZIF, Heidelberg, Germany). We also do not have such information.
Population characteristics	For the in vitro culture studies: we used PBMC from healthy volunteers from 24 to 69 years of age. For the HIV patient tissue section studies: lymph node sections were provided by the tissue bank of the German Center for Infection Research. Donors were 34 to 74 years of age.
Recruitment	For the in vitro culture studies: Buffy coat PBMC samples from healthy donors were provided by the blood bank of Mannheim, Germany. When choosing samples, we have considered both age (from 18 to 70 years of age) and gender (both male and female), but we did not consider other factors, such as race, ethnicity, or other socially relevant groupings. For the HIV patient tissue section studies: lymph node sections were provided by the tissue bank of the German Center for Infection Research (DZIF, Heidelberg, Germany). Samples were chosen based on HIV positive or negative irrespective of age, gender, ethnicity or any other bias that could influence study outcomes.
Ethics oversight	This study was performed in accordance with the approval of the ethics committee of Heidelberg University.

Note that full information on the approval of the study protocol must also be provided in the manuscript.

Field-specific reporting

Please select the one below that is the best fit for your research. If you are not sure, read the appropriate sections before making your selection.

☒ Life sciences ☐ Behavioural & social sciences ☐ Ecological, evolutionary & environmental sciences

For a reference copy of the document with all sections, see nature.com/documents/nr-reporting-summary-flat.pdf

Life sciences study design

All studies must disclose on these points even when the disclosure is negative.

Sample size	No formal statistical methods were used to predetermine sample sizes but our sample sizes are similar to those reported in previous publications

Data exclusions	We did not exclude data.
Replication	Experiments were repeated twice or three times, as indicated in the figure legends.
Randomization	For the comparison between wildtype and knockout mice, littermate mice were allocated into 2 groups based on genotypes (namely wildtype and knockout mice). For the P14 T cell adoptive transfer experiments, C57Bl/6N mice were randomly allocated into different groups. We did not use a randomization protocol for the rest of the experiments.
Blinding	Data collection and analysis were not performed blind to the conditions of the experiments, because investigators who planned the experiments also performed them.

Reporting for specific materials, systems and methods

We require information from authors about some types of materials, experimental systems and methods used in many studies. Here, indicate whether each material, system or method listed is relevant to your study. If you are not sure if a list item applies to your research, read the appropriate section before selecting a response.

Materials & experimental systems

n/a	Involved in the study
☐	☒ Antibodies
☒	☐ Eukaryotic cell lines
☒	☐ Palaeontology and archaeology
☐	☒ Animals and other organisms
☒	☐ Clinical data
☒	☐ Dual use research of concern
☒	☐ Plants

Methods

n/a	Involved in the study
☒	☐ ChIP-seq
☐	☒ Flow cytometry
☒	☐ MRI-based neuroimaging

Antibodies

Antibodies used

Anti-GOT1 (clone E4A4O), Cell Signaling Technology, Cat# 34423S, dilution: 1:500 for flow cytometry and tissue section stainings; 1:1000 for immunoblotting
Alexa Fluor 488-conjugated donkey anti-rabbit secondary antibody, BioLegend, Cat# 406416, dilution: 1:2000
Alexa Fluor 647-conjugated anti-CD8a (clone C8/144B), BioLegend, Cat# 372906, dilution: 1:200
Anti-GRP94 (clone D6X2Q), Cell Signaling Technology, Cat# 20292, dilution: 1:500 for immunoblotting
Anti-NFAT1 (clone D43B1), Cell Signaling Technology, Cat# 5861, dilution: 1:200 for ChIP
Anti-TOX, polyclonal, Abcam, Cat# ab155768, dilution: 1:200 for ChIP
Anti-Eomes, polyclonal, Cell Signaling Technology, Cat# 4540, dilution: 1:200 for ChIP
Anti-Blimp1 (clone C14A4), Cell Signaling Technology, Cat# 9115, dilution: 1:200 for ChIP
Rabbit IgG, polyclonal, Cell Signaling Technology, Cat# 2729, dilution: 1:200 for ChIP
Brilliant Violet 421™ anti-mouse CD8a Antibody (clone 53-6.7), BioLegend, Cat# 100738, dilution: 1:200
PE Donkey anti-rabbit IgG (minimal x-reactivity) Antibody, polyclonal, BioLegend, Cat# 406421, dilution: 1:1000
PerCP/Cyanine5.5 anti-mouse CD8a Antibody (clone 53-6.7), BioLegend, Cat# 100734, dilution: 1:200
Brilliant Violet 711™ anti-mouse CD45.1 Antibody (clone A20), BioLegend, Cat# 110739, dilution: 1:400
PE anti-mouse TIGIT (Vstm3) Antibody (clone 1G99), BioLegend, Cat# 142104, dilution: 1:400
PE/Cyanine7 anti-mouse CD279 (PD-1) Antibody (clone 29F.1A12), BioLegend, Cat# 135216, dilution: 1:400
PE anti-mouse TNF-α Antibody (clone MP6-XT22), BioLegend, Cat# 506306, dilution: 1:400
PE/Cyanine7 anti-mouse IFN-γ Antibody(clone XMG1.2), BioLegend, Cat# 505826, dilution: 1:400
Bim Rabbit mAb (Alexa Fluor® 488 Conjugate) (clone C34C5), Cell Signaling Technology, Cat# 94805, dilution: 1:400
Cleaved Caspase-3 (Asp175) Rabbit mAb (clone 5A1E), Cell Signaling Technology, Cat# 9664, dilution: 1:400
Brilliant Violet 421™ Donkey anti-rabbit IgG (minimal x-reactivity) Antibody, polyclonal, BioLegend, Cat# 406410, dilution: 1:1000
Ki-67 Antibody, anti-human/mouse, PE-Vio® 770, REAfinity™ (clone REA183), Miltenyi Biotec., Cat# 130-120-419, dilution: 1:400
Brilliant Violet 421™ anti-mouse CD4 Antibody (clone GK1.5), BioLegend, Cat# 100438, dilution: 1:200
APC/Cyanine7 anti-mouse CD4 Antibody (clone GK1.5), BioLegend, Cat# 100414, dilution: 1:200
Brilliant Violet 421™ anti-mouse/human CD44 Antibody (clone IM7), BioLegend, Cat# 103040, dilution: 1:400PE/Cyanine7 anti-mouse CD62L Antibody (clone MEL-14), BioLegend, Cat# 104418, dilution: 1:400
APC anti-mouse CD25 Antibody (clone 3C7), BioLegend, Cat# 101910, dilution: 1:400
PE anti-mouse CD127 (IL-7Rα) Antibody (clone A7R34), BioLegend, Cat# 135010, dilution: 1:400
Ultra-LEAF™ Purified anti-mouse CD16/32 Antibody (clone 93), BioLegend, Cat# 101330, dilution: 1:100
Ultra-LEAF™ Purified anti-mouse CD3 Antibody (clone 17A2), BioLegend, Cat# 100238, dilution: 2 ug/ml
Ultra-LEAF™ Purified anti-mouse CD28 Antibody (clone 37.51), BioLegend, Cat# 102116, dilution: 2 ug/ml
Ultra-LEAF™ Purified anti-human CD3 Antibody (clone OKT3), BioLegend, Cat# 317326, dilution: 2 ug/ml
Ultra-LEAF™ Purified anti-human CD2 Antibody (clone TS1/8), BioLegend, Cat# 309236, dilution: 2 ug/ml
Ultra-LEAF™ Purified anti-human CD28 Antibody (clone CD28.2), BioLegend, Cat# 302934, dilution: 2 ug/ml

Validation

Anti-GOT1 https://www.cellsignal.com/products/primary-antibodies/got1-e4a4o-rabbit-mab/34423
Alexa Fluor 488-conjugated donkey anti-rabbit secondary antibody https://www.biolegend.com/fr-lu/products/alexa-fluor-488-

donkey-anti-rabbit-igg-minimal-x-reactivity-9380
Alexa Fluor 647-conjugated anti-CD8a https://www.biolegend.com/en-gb/products/alexa-fluor-647-anti-human-cd8a-antibody-14127?GroupID=BLG15860
Anti-GRP94 https://www.cellsignal.com/products/primary-antibodies/grp94-d6x2q-xp-rabbit-mab/20292
Anti-NFAT1 https://www.cellsignal.com/products/primary-antibodies/nfat1-d43b1-xp-rabbit-mab/5861
Anti-TOX https://www.abcam.com/products/primary-antibodies/tox-antibody-ab155768.html
Anti-Eomes https://www.cellsignal.com/products/primary-antibodies/eomes-antibody/4540
Anti-Blimp1 https://www.cellsignal.com/products/primary-antibodies/blimp-1-prdi-bf1-c14a4-rabbit-mab/9115
Rabbit IgG https://www.cellsignal.com/products/primary-antibodies/normal-rabbit-igg/2729
Brilliant Violet 421™ anti-mouse CD8a Antibody https://www.biolegend.com/fr-fr/search-results/brilliant-violet-421-anti-mouse-cd8a-antibody-7138
PE Donkey anti-rabbit IgG (minimal x-reactivity) Antibody https://www.biolegend.com/fr-fr/products/pe-donkey-anti-rabbit-igg-minimal-x-reactivity-9751
PerCP/Cyanine5.5 anti-mouse CD8a Antibody https://www.biolegend.com/en-us/products/percp-cyanine5-5-anti-mouse-cd8a-antibody-4255
Brilliant Violet 711™ anti-mouse CD45.1 Antibody https://www.biolegend.com/en-us/products/brilliant-violet-711-anti-mouse-cd45-1-antibody-8925
PE anti-mouse TIGIT (Vstm3) Antibody https://www.biolegend.com/en-us/products/pe-anti-mouse-tigit-vstm3-antibody-7429
PE/Cyanine7 anti-mouse CD279 (PD-1) Antibody https://www.biolegend.com/en-us/products/pe-cyanine7-anti-mouse-cd279-pd-1-antibody-7005
PE anti-mouse TNF-α Antibody https://www.biolegend.com/en-us/products/pe-anti-mouse-tnf-alpha-antibody-978
PE/Cyanine7 anti-mouse IFN-γ Antibody https://www.biolegend.com/en-us/products/pe-cyanine7-anti-mouse-ifn-gamma-antibody-5865
Bim Rabbit mAb (Alexa Fluor® 488 Conjugate) https://www.cellsignal.com/products/antibody-conjugates/bim-c34c5-rabbit-mab-alexa-fluor-488-conjugate/94805
Cleaved Caspase-3 (Asp175) Rabbit mAb (clone 5A1E) https://www.cellsignal.com/products/primary-antibodies/cleaved-caspase-3-asp175-5a1e-rabbit-mab/9664
Brilliant Violet 421™ Donkey anti-rabbit IgG (minimal x-reactivity) Antibody https://www.biolegend.com/en-us/products/brilliant-violet-421-donkey-anti-rabbit-igg-minimal-x-reactivity-7262
Ki-67 Antibody, anti-human/mouse, PE-Vio® 770, REAfinity™ https://www.miltenyibiotec.com/DE-en/products/ki-67-antibody-anti-human-mouse-reafinity-rea183.html#conjugate=pe-vio-770:size=100-tests-in-200-ul
Brilliant Violet 421™ anti-mouse CD4 Antibody https://www.biolegend.com/en-us/products/brilliant-violet-421-anti-mouse-cd4-antibody-7142
APC/Cyanine7 anti-mouse CD4 Antibody https://www.biolegend.com/en-us/products/apc-cyanine7-anti-mouse-cd4-antibody-1964
Brilliant Violet 421™ anti-mouse/human CD44 Antibody https://www.biolegend.com/en-us/products/brilliant-violet-421-anti-mouse-human-cd44-antibody-7225
PE/Cyanine7 anti-mouse CD62L Antibody https://www.biolegend.com/en-us/products/pe-cyanine7-anti-mouse-cd62l-antibody-1922
APC anti-mouse CD25 Antibody https://www.biolegend.com/en-us/products/apc-anti-mouse-cd25-antibody-4512
PE anti-mouse CD127 (IL-7Rα) Antibody https://www.biolegend.com/en-us/products/pe-anti-mouse-cd127-il-7ralpha-antibody-6190
Ultra-LEAF™ Purified anti-mouse CD16/32 Antibody https://www.biolegend.com/en-us/products/ultra-leaf-purified-anti-mouse-cd16-32-antibody-8081
Ultra-LEAF™ Purified anti-mouse CD3 Antibody https://www.biolegend.com/en-us/products/ultra-leaf-purified-anti-mouse-cd3-antibody-8078
Ultra-LEAF™ Purified anti-mouse CD28 Antibody https://www.biolegend.com/en-us/products/ultra-leaf-purified-anti-mouse-cd28-antibody-7733
Ultra-LEAF™ Purified anti-human CD3 Antibody https://www.biolegend.com/en-us/products/ultra-leaf-purified-anti-human-cd3-antibody-7745
Ultra-LEAF™ Purified anti-human CD2 Antibody https://www.biolegend.com/en-us/search-results/ultra-leaf-purified-anti-human-cd2-antibody-19172?GroupID=BLG9913&gclid=CjwKCAjwoqGnBhAcEiwAwK-OkVkQoC2W8tSgy4348nJzJKM89IWKrggBopxNoAuUv8Ia8Eq2PbyAaxoCjUEQAvD_BwE
Ultra-LEAF™ Purified anti-human CD28 Antibody https://www.biolegend.com/en-us/products/ultra-leaf-purified-anti-human-cd28-antibody-7743

Animals and other research organisms

Policy information about studies involving animals; ARRIVE guidelines recommended for reporting animal research, and Sex and Gender in Research

Laboratory animals	Mice were maintained in the German cancer research center (DKFZ) specific pathogen-free facility. The Got1Flox/Flox mice, under the full name C57BL/6N-Got1tm1c(EUCOMM)Hmgu/H, were ordered from the MRC Harwell Institute, Oxfordshire, UK. Exon 2 of Got1 is flanked by two LoxP sites and is excised after crossing with a Cre-expression mouse strain. Cd4-Cre mice and P14 mice were from The Jackson Laboratory and have been backcrossed to C57BL/6N background for more than 10 generations. Mice were housed with a 12-h day–night cycle in a controlled environment at 20–24 °C and 45–65% humidity, and were fed a regular chow diet (cat#3437, Kliba Nafag) ad libitum. In rare cases, mice with fighting wounds were excluded from the experimental analysis. The sample collection and processing were not performed in a blinded manner.
Wild animals	We did not use wild animals.
Reporting on sex	We used both male and female mice in this study. We used sex-matched mice for each individual experiment.
Field-collected samples	No field-collected samples were used.
Ethics oversight	All studies were performed in accordance with DKFZ regulations with approval by the German regional council at the

Ethics oversight | Regierungspräsidium Karlsruhe (G-232/16).

Note that full information on the approval of the study protocol must also be provided in the manuscript.

Flow Cytometry

Plots

Confirm that:

☒ The axis labels state the marker and fluorochrome used (e.g. CD4-FITC).

☒ The axis scales are clearly visible. Include numbers along axes only for bottom left plot of group (a 'group' is an analysis of identical markers).

☒ All plots are contour plots with outliers or pseudocolor plots.

☒ A numerical value for number of cells or percentage (with statistics) is provided.

Methodology

Sample preparation	Spleens were smashed using a syringe through a 70 um cell strainer. For surface antigen staining, Fc receptor blockers anti-CD16/CD32 were used to prevent nonspecific antibody binding. Cells were incubated in FACS buffer (PBS supplemented with 0.5% FCS) with the fluorescently conjugated antibodies for 30 minutes on ice. DAPI or a Live/DEAD Fixable Dead Cell Stain kit (Thermo Fisher) was used to exclude the dead cells. For intracellular cytokine staining, cells were fixed with the fixation buffer containing 4% paraformaldehyde (PFA; BioLegend) first, then permeabilized with eBioscience permeabilization buffer. For staining nuclear antigens, cells were fixed and permeabilized with the eBioscience Foxp3/transcription factor staining buffer set on ice for at least 30 minutes.
Instrument	Samples were washed and run on an LSR II or LSR Fortessa flow cytometer.
Software	We used FACS Diva Software (version 9, BD Biosciences) to collect FACS data and analyzed data in FlowJo software (10.1r1).
Cell population abundance	FACS sorting had a purity> 95%, which was confirmed by post-sort FACS analysis.
Gating strategy	Gates were first set based on FSC-A/SSC-A and doublets were excluded using FSC-H and FSC-A. Life/death dye was used to exclude dead cells. T cells were then gated for further analysis.

☒ Tick this box to confirm that a figure exemplifying the gating strategy is provided in the Supplementary Information.